AD-A086 074 OHIO STATE UNIV COLUMBUS ELECTROSCIENCE LAB F/G 9/5
A HYBRID MOMENT METHOD - GTD TECHNIQUE FOR ANALYSIS OF ANTENNAS--ETC(U)
APR 80 L W HENDERSON, G A THIELE N00014-78-C-0049
UNCLASSIFIED ESL-710816-7 NL

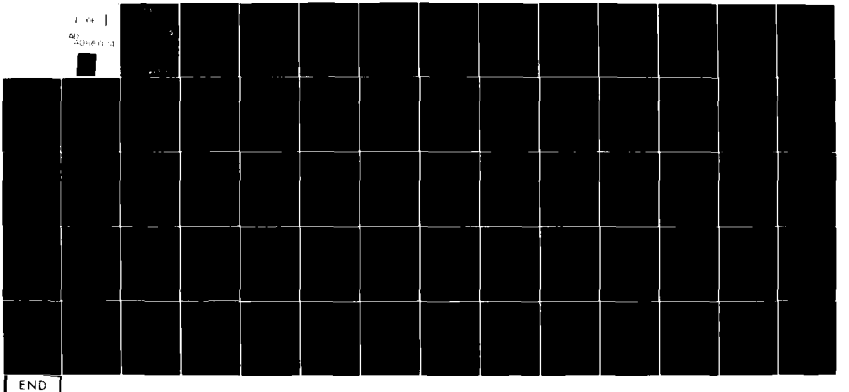

END
DATE FILMED
8-80
DTIC

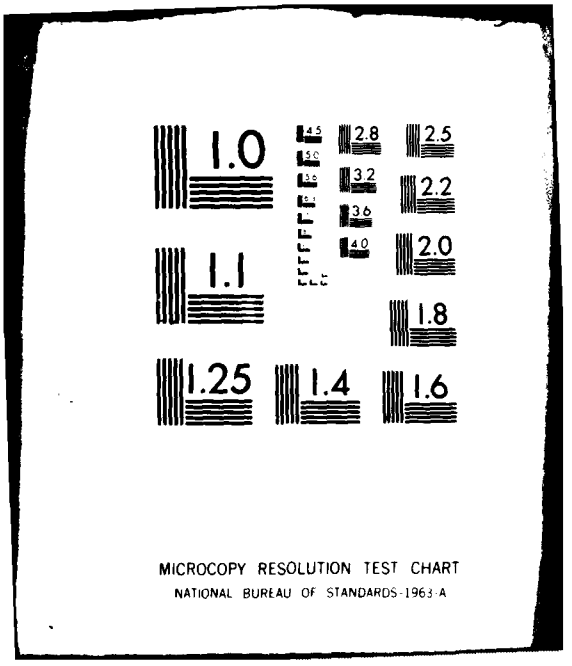
1.0
1.1
1.25
1.4
1.6
1.8
2.0
2.2
2.5
2.8
3.2
3.6
4.0
4.5
5.0
5.6
MICROCOPY RESOLUTION TEST CHART
NATIONAL BUREAU OF STANDARDS-1963-A

LEVEL II

13

OSU

A HYBRID MOMENT METHOD - GTD TECHNIQUE FOR ANALYSIS OF ANTENNAS MOUNTED ON OR NEAR CURVED SURFACES

Lee M. Henderson and Gary A. Thiele

The Ohio State University

The Ohio State University

ElectroScience Laboratory

Department of Electrical Engineering

Columbus, Ohio 43212

Technical Report 711816-7

Contract N00014-78-C-0049

April 1980

NOTICES

When Government drawings, specifications, or other data are used for any purpose other than in connection with a definitely related Government procurement operation, the United States Government thereby incurs no responsibility nor any obligation whatsoever, and the fact that the Government may have formulated, furnished, or in any way supplied the said drawings, specifications, or other data, is not to be regarded by implication or otherwise as in any manner licensing the holder or any other person or corporation, or conveying any rights or permission to manufacture, use, or sell any patented invention that may in any way be related thereto.

SECURITY CLASSIFICATION OF THIS PAGE (When Data Entered)

REPORT DOCUMENTATION PAGE

READ INSTRUCTIONS BEFORE COMPLETING FORM

1. REPORT NUMBER	2. GOVT ACCESSION NO. AD-A086074
	3. RECIPIENT'S CATALOG NUMBER
4. TITLE (and Subtitle) (6) A HYBRID MOMENT METHOD - GTD TECHNIQUE FOR ANALYSIS OF ANTENNAS MOUNTED ON OR NEAR CURVED SURFACES.	5. TYPE OF REPORT & PERIOD COVERED (9) Technical Report. (16)
	6. PERFORMING ORG. REPORT NUMBER (14) ESL-710916-7
7. AUTHOR(s) (10) Lee W. Handerson and Gary A. Thiele	8. CONTRACT OR GRANT NUMBER(s) Contract N00014-78-C-0049 (15)
9. PERFORMING ORGANIZATION NAME AND ADDRESS The Ohio State University ElectroScience Laboratory, Department of Electrical Engineering, Columbus, Ohio 43212	10. PROGRAM ELEMENT, PROJECT, TASK AREA & WORK UNIT NUMBERS Project NR 371-021/9-5-78 (427)
11. CONTROLLING OFFICE NAME AND ADDRESS Dept. of the Navy, Office of Naval Research, 800 Quincy Street Arlington, Virginia 22217 (11)	12. REPORT DATE Apr 80
	13. NUMBER OF PAGES 63
14. MONITORING AGENCY NAME & ADDRESS (if different from Controlling Office) (12) 68	15. SECURITY CLASS. (of this report) Unclassified
	15a. DECLASSIFICATION/DOWNGRADING SCHEDULE

16. DISTRIBUTION STATEMENT (of this Report)

This document has been approved for public release and sale; its distribution is unlimited.

17. DISTRIBUTION STATEMENT (of the abstract entered in Block 20, if different from Report)

18. SUPPLEMENTARY NOTES

The material contained in this report is also used as a thesis submitted to the Department of Electrical Engineering, The Ohio State University as partial fulfillment for the degree Master of Science.

19. KEY WORDS (Continue on reverse side if necessary and identify by block number)

Moment method
Diffraction theory
Geometrical Theory of Diffraction
Hybrid technique
Mutual coupling
Antennas
Electromagnetic scattering

20. ABSTRACT (Continue on reverse side if necessary and identify by block number)

A hybrid technique which will analyze thin wire scatterers in the presence of a large conducting body is presented. This technique is quite general and applicable to a large class of problems. Two specific cases were chosen to demonstrate the usefulness of this approach. The first example given is of two piecewise sinusoidal dipoles

DD FORM 1 JAN 73 1473 EDITION OF 1 NOV 65 IS OBSOLETE

SECURITY CLASSIFICATION OF THIS PAGE (When Data Entered)

402251

20.

arbitrarily positioned near an infinite, perfectly conducting cylinder. The second example provides a method for analyzing antennas mounted on the cylinder, such as a monopole. This solution is obtained as a perturbation of image theory.

TABLE OF CONTENTS

CHAPTER I
INTRODUCTION

In recent years many new techniques have been developed for analyzing systems which could not be adequately handled by classical methods. Two of the most powerful of these theories are the moment method (MM) and the geometrical theory of diffraction (GTD). The moment method is a variational technique for solving integral equations by reducing them to a system of N algebraic equations with N unknown coefficients. Since most electromagnetic scattering problems can be formulated as an integral equation, the moment method finds wide application. Due to the fact that the number of unknowns is more or less directly related to the size of the scattering system, the moment method is usually limited to systems which are not electrically large.

The GTD is an asymptotic technique which takes advantage of the fact that electromagnetic radiation behaves as a ray optical phenomenon. The usefulness of GTD rests on the idea that interaction between rays and objects are local occurances and thus it is not necessary to integrate currents over an entire structure as is done in classical techniques. This local nature of the interaction, allows complex geometries to be built from canonical forms such as flat plates, cylinders, wedges, cones, etc. However, because of its asymptotic formulation, GTD is primarily useful for systems which are electrically large. Thus there exists a gap in the tools available for analyzing scattering systems. Systems which contain an electrically small scatterer in the presence of a large body cannot be adequately analyzed by either the moment method or GTD

The hybrid method presented in this paper presents a technique for analyzing such a system. The work, presented herein is based on previous papers by Thiele and Newhouse [7] and by Ekelman [1]. The approach taken is to cast the small scatterer (built of thin wires) in the moment method format of Richmond [8] and then add perturbation terms due to interaction with the nearby large body using GTD. Thus the solution is basically a GTD perturbation of the moment method. The particular form of the GTD used in this work is a new ansatz called the uniform theory of diffraction (UTD) reported by Pathak et al [3]. The UTD avoids previous difficulties encountered with GTD when a ray hits a curved edge at grazing incidence.

The hybrid method is a general technique which is applicable to a large class of problems. The particular solutions presented herein extend the initial work done by Ekelman, providing further examples of the utility of the hybrid technique and greatly broaden the scope of problems for which solutions are currently available. The first solution given is for two piecewise sinusoidal dipoles arbitrarily positioned around an infinite circular cylinder. This, along with Richmond's work, provides a technique for analyzing any arbitrary combination of thin wire antennas near a conducting cylinder. The second solution provides a method for analyzing antennas mounted on the cylinder, such as a monopole. This solution is obtained as a perturbation of image theory. This monopole solution is, in principle, as general as the rest of the hybrid theory, however the GTD expression needed for a completely general monopole analysis were not available. Thus the data presented does not include the full GTD.

Chapter II contains the development of the moment method as it is used in this work. Chapter III presents the essential points of the GTD (UTD) and included the UTD expressions of Pathak et al. The hybrid method is covered in detail in Chapter IV. Results of the two dipole problem are presented in Chapter V and Chapter VI contains the theory and implementation notes on the monopole problem from conclusing remarks are contained in Cahpter VII.

CHAPTER II
THE MOMENT METHOD

The moment method is a procedure for solving an integral equation of the first kind as in Equation (1)

$$\int I(\bar{r}')K(\bar{r},\bar{r}')d\bar{r}' = -E^i(\bar{r}) \qquad (1)$$

over a structure

Almost all electromagnetic scattering problems can be put into the form of Equation (1) and then, in principle, solved by moment-method techniques. Since the moment method is such an extremely powerful mathematical tool, a completely general discussion would be quite abstract and thus not entirely suitable for the purposes of this paper. We will therefore consider a specialized case of the moment method. We will consider an arbitrary structure built from electrically thin wires (wire radius $< .006\lambda$). Since a large portion of antennas in common use today are made of or can be modeled by thin wires, this solution will be applicable to a large class of problems. For such a structure, the scattering is given by Pocklington's integral equation (2) for a z directed segment

$$\frac{1}{j\omega\varepsilon_0}\int_{\text{over structure}} I(z')[\nabla^2 G(z,z') + \beta^2 G(z,z')]dz' = -E_s^i(z) \qquad (2)$$

where G(z,z') is the free space Green's function

$$G(z,z') = \frac{e^{-j\beta|z-z'|}}{|z-z'|} \qquad (3)$$

The function I(z') is the current in the wires and $E_s^i(z)$ is the incident or impressed field at the surface of the wire.

Note that the volume integral of (1) has become a line integral in (2) since the current on a thin wire is assumed to be a line source. A typical example of the type of problem which can be solved by (2) is shown in Figure 1 where a thin wire h wavelengths long ($h<<1$) is illuminated by a plane wave The quantity $E_s^i(z)$ is the electric field incident on the wire and I(z) is the unknown currents induced by the incident field.

The simple example in Figure 1 can be solved by assuming a current

$$I(z) = \frac{I_0 \sin\eta(\frac{h}{2} - |z|)}{\sin(\frac{\eta h}{2})} \tag{4}$$

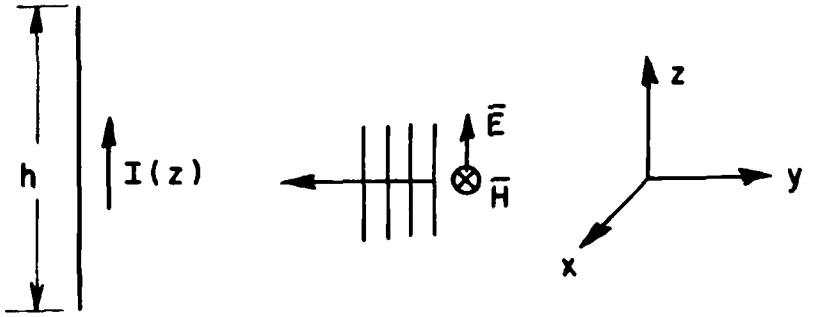

Figure 1. Thin wire illuminated by a plane wave.

Substituting (4) into (2) along with the known function $E_s^i(z)$ will give I_o and thus the problem is solved. For a more complex structure, the form of the current is not known and thus no assumption can be made as in (4), in this situation the moment method is used.

The moment-method technique produces numerical solution to an equation such as (2) by transforming the integral equation into a set of linear algebraic equations as follows. Consider an arbitrary, complex thin wire structure. The unknown currents on such a structure can be expanded as a series of expansion functions

$$I(z) = \sum_{n=1}^{N} I_n J_n(z) \tag{5}$$

where the expansion functions $J_n(z)$ are arbitrarily chosen (as in the example for Figure 1) and defined over a particular portion of the structure, and zero elsewhere. These functions along with the weighting coefficients I_n, describe an arbitrary current distribution as $N \to \infty$. Obviously, for numerical computation it is desireable to make N as small as possible and still obtain accurate results. The choice of J_n will be discussed shortly.

Substituting (5) into (1) gives

$$\oint \sum_{n=1}^{N} I_n J_n(z')K(z,z')dz' = -E_x^i(z) \tag{6}$$

Now all of the terms inside the integral are known, and thus the integral can be evaluated to give

$$\sum_{N=1}^{N} I_n F_n(z) = -E_s^i(z) \tag{7}$$

where

$$F_n(z) = \oint J_n(z)K(z,z')dz' \tag{8}$$

Now the integral has been removed but the result is one equation with (N) unknown. The (N) equation needed to solve (7) and be produced using weighted residuals.

Weighted Residuals

The well known boundary conditions at the surface of a perfectly conducting wire are

$$\bar{E}_T^i = -\bar{E}_T^s \tag{9}$$

where $\bar{E}_T^i$ and $\bar{E}_T^s$ are respectively the tangential incident and scattered fields. Since the assumed form of the current (Equation (5)) is in general not exact unless N=∞, then the residual defined in Equation (10) will not be zero

$$R(z) = E_T^s(z) + E_T^i(z) \tag{10}$$

for all z.

In order to preserve the boundary condition as nearly as possible, the residual is forced to zero in an average sense. It is hoped that in so doing, the result will be as near to the exact answer as possible. Using a weighted average gives,

$$\int_{\text{over structure}} W_m(z)R(z)dz = 0 \quad \int n=1,2,3.. \tag{11}$$

here $W_m(z)$ are arbitrary weighting functions. The choice of these will be discussed shortly.

Substituting (11) and (10) into (7) gives

$$\int_{\text{over structure}} W_m(z) \sum_{n=1}^{N} I_n F_n(z)dz = \int_{\text{over structure}} E_s^i(z)W_m(z)dz \tag{12}$$

$$m = 1,2,...N$$

which will yield the required N equations. Equation (12) can be written in a simpler form by substituting

$$V_m = -\int_{\text{over structure}} E_s^i(z)W_m(z)\,dz \tag{13}$$

$$Z_{mn} = \int_{\text{over structure}} W_m(z)F_n(z)dz \tag{14}$$

Then

$$\sum_{n=1}^{N} I_n Z_{mn} = V_m \qquad m=1,2,...N \tag{15}$$

or in matrix notation

$$[V] = [Z][I\ ] \tag{16}$$

Obviously (16) can be solved by suitable techniques, thus yielding the required coefficients (I_n).

The choice of $J_n(z)$ and $W_m(z)$ have a great deal to do with the number of terms (N) needed to get an accurate result. In general the more closely these functions model the actual current distribution on the wire, the smaller (N) can be. When $J_n(z)$ and $W_m(z)$ are the same, one obtains a special case of the moment method called Galerkin's method.

The Reaction Integral

The preceeding development of the moment method, while mathematically correct, gives little physical insight into the quantities Z_{mn} and V_m (Equations (13), (14)). These quantities can be shown to have physical significance as follows.

In 1954, Rumsey[11] introduced a physical observable called reaction, as

$$\iint_S (J_m \cdot E_s - M_m \cdot H_s)ds - \iint_S J_m \cdot E_i - M_m \cdot H_i)ds = 0 \qquad (17)$$

where (E_s, H_s) denotes the field generated by the equivalent surface current densities $(J_s\ M_s)$ of a test source $(J_m\ M_m)$, as in Figure 2. Also (E_i, H_i) are the fields of an external source $(J^i\ M^i)$. Physically, Equation (17) states that there is zero reaction or coupling between the test source and the sum of the incident and scattered fields. This is equivalent to the weighted residual interpretation of Equation (11). For the case of thin wires and electric currents, $M_m = 0$ and the surface integrals reduce to line integrals, thus (17) becomes

$$\int(\bar{J}_m \cdot \bar{E}_s)dz = \int (\bar{J}_m \cdot \bar{E}_i)ds \qquad (18)$$

which is the same form as (12). Thus the weight function can be interpreted as test currents or test sources. If the expansion functions are taken to be at the center of the perfectly conducting wires, and the surface s in Figure 2 is taken to be the surface of the wire, then Z_{mn} is merely the coupling between the mth test function and the nth expansion function.

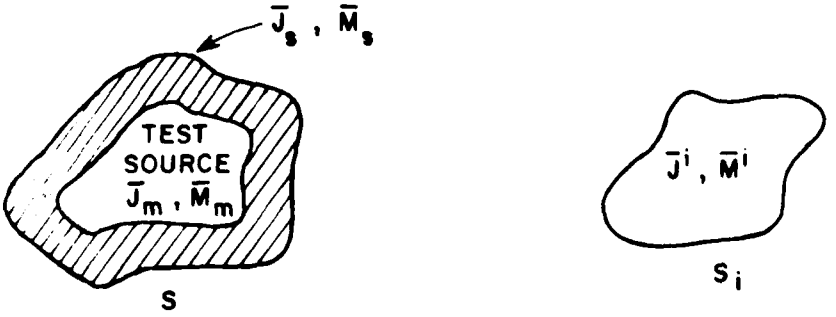

Figure 2. Test source $(\bar{J}_m, \bar{M}_m)$ inside conducting body surface S.

Piecewise Sinusoidal Galerkin Method

The piecewise sinusoid, Figure 3, used by Richmond [8]is one of the most useful basis functions for thin wires. It may be expressed mathematically for each z-directed segment by

$$I(z) = \frac{I_1 \sinh\gamma(z_2-z)+I_2\sinh\gamma(z-z_1)}{\sin\gamma d} \tag{19}$$

where I_1 and I_2 are the endpoint currents, γ is the complex propagation constant of the medium, and $d=z_2-z_1$ is the source length. Piecewise sinusoids are efficient since very few are needed to approximate the expected current distribution as in Figure 4.

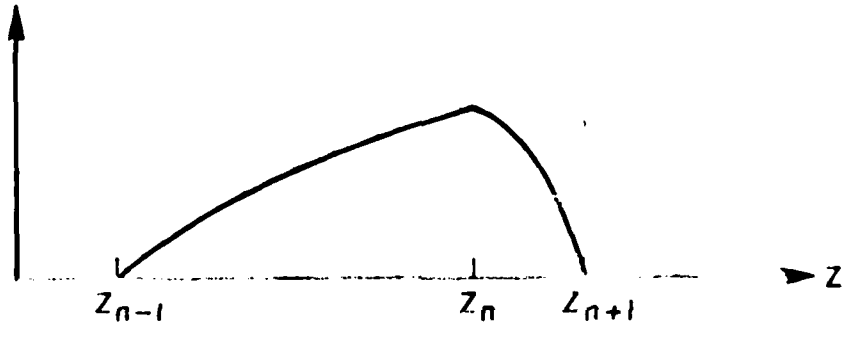

Figure 3. Typical two segment dipole with piecewise sinusoidal distribution.

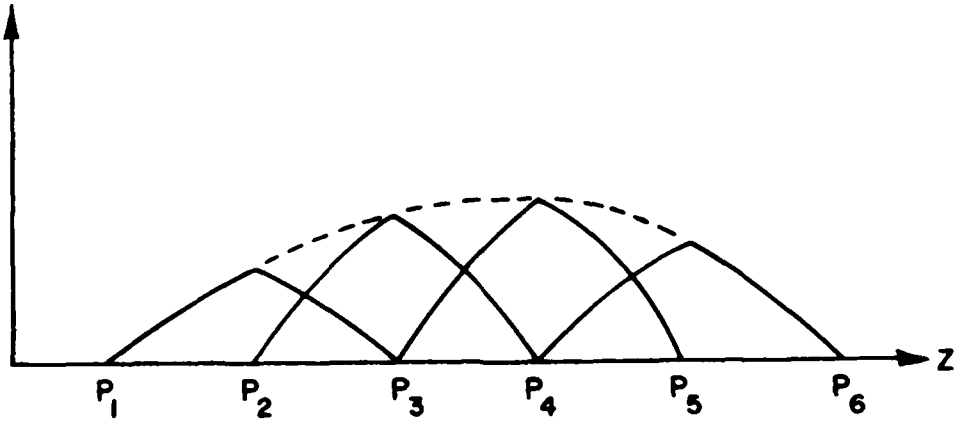

Figure 4. Current distribution modeled by overlapping piecewise sinusoidal modes.

Note that each piecewise sinusoid function spans two connected segments and that each interior segment contains two piecewise sinusoidal functions. Thus it is convenient to consider each piecewise sinusoid as a dipole with its source at the junction between the segments. Consider the situation wherein an arbitrary number of segments are coincident with the z-axis. For example, for an antenna with N segments, the mn-th impedance matrix element is

$$Z_{mn} = \int_{z_{m-1}}^{z_m} \frac{\sin(z-z_{m-1})}{\sin|z_{m-1}-z_m|} \hat{z}\cdot\bar{E}_n^s dz + \int_{z_m}^{z_{m+1}} \frac{\sin(z_{m+1}-z)}{\sin|z_m-z_{m+1}|} \hat{z}\cdot\bar{E}_n^s dz. \quad (20)$$

The field $\bar{E}_n^s$ needed to evaluate Equation (20) may be found in a straightforward manner, and the derivation is included in many electromagnetic texts including [9]. The geometry is shown in Figure 5. For the piecewise sinusoidal excitation current $\bar{E}_n^s$ is

$$E_\rho = \frac{n}{4\pi\rho\sinh\gamma d}\left[\left(I_1 e^{-\gamma R_1} - I_2 e^{-\gamma R_2}\right)\sinh\gamma d + (I_1\cosh I - I_2)e^{-\gamma R_1}\cos\theta_1 + (I_2\cosh d - I_1)e^{-\gamma R_2}\cos\theta_2\right] \quad (21)$$

$$E_z = \frac{n}{4\sinh\gamma d}\left[(I_1 - I_2\cosh d)\frac{e^{-\gamma R_2}}{R_2} + (I_2 - I_1\cosh d)\frac{e^{-\gamma R_1}}{R_1}\right] \quad (22)$$

where n is the impedance of the medium. The evaluation of Equation (20) may be carried out without difficulty by numerical integration or by Si and Ci integrals for some special geometries.

The piecewise sinusoidal Galerkin method presented here is the procedure used for the thin-wire antennas of this paper. The importance of this particular specialization of the moment method for the hybrid technique will be discussed in Chapter IV.

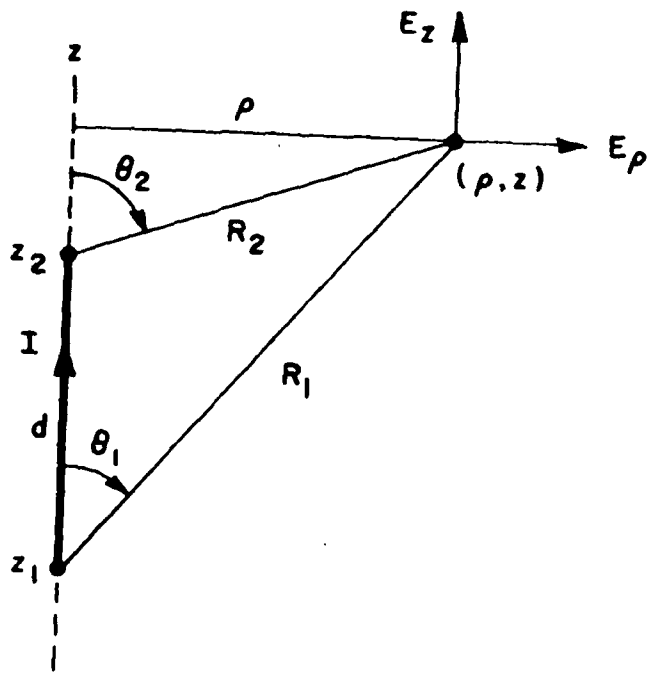

Figure 5. z-directed monopole segment source with the observation point (ρ,z).

CHAPTER III
GEOMETRICAL THEORY OF DIFFRACTION

While the moment method is a technique primarily for low frequency, the geometrical theory of diffraction (GTD) is useful for high frequency, or situations where the scatterer is electrically large. The foundation of GTD rests on two basic principles.

i. Electromagnetic propagation is a ray type phenomenon, that is, a wave travelling from point a in space to point b, will follow a geodesic path. In general, there is more than one such path and the contribution from all such paths must be considered before an accurate solution can be reached. Several examples are shown in Figure 6.

ii. Secondly, all interaction between rays and objects are localized phenomenon. Thus it is not necessary to integrate the currents over an entire structure in order to obtain the scattered field. It is only necessary to determine the incident ray and the geometry of the object at the points where the ray is in "contact" with the surface.

The localized nature of the interaction and the ray optic scattering at once enable one to model a complex structure from simple geometric shapes, such as cylinders and plates. Once this model has been constructed one can quickly evaluate the components of the structure which will have a significant effect on the scattered field. For most structures there are an infinite number of geodesic ray paths from point a to point b, however the nature of the diffraction allows one to quickly determine the significant rays in order to arrive at an engineering solution. Assuming the scatterer does not hide the source, the dominant field is produced by the direct ray from the source to the observer. The next most important term is the ray reflected from the scatterer. This field is termed the geometrical optics field.

A. The Geometrical Optics Field

Although the GTD can handle a general astigmatic wave front, only spherical waves will be discussed here for reasons that will

REFLECTION

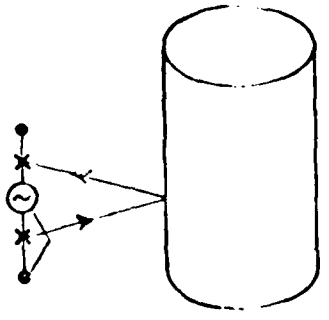

EDGE DIFFRACTION

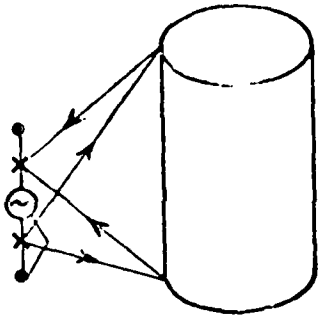

CREEPING WAVE

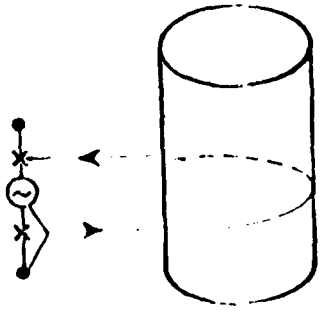

Figure 6. Scattering mechanisms for dipole interaction with cylinder.

be apparent later. The geometry, shown in Figure 7, consists of an arbitrarily curved smooth, perfectly conducting surface with nearby source and observation points. The ray path is from the source point to the reflection point, and then to the observation point. The reflected field $E^r(s)$ of a curved surface S is

$$E^r(s) = E^i(Q_R) \cdot \bar{\bar{R}} \sqrt{\frac{\rho_1^r \rho_2^r}{(\rho_1^r+s)(\rho_2^r+s)}} \; e^{-jks} \tag{23}$$

where $E^i(Q_R)$ is the incident field at the reflection point Q_R. In (23), as in all of the formulas given, the $e^{j\omega t}$ time dependence is assumed but not shown.

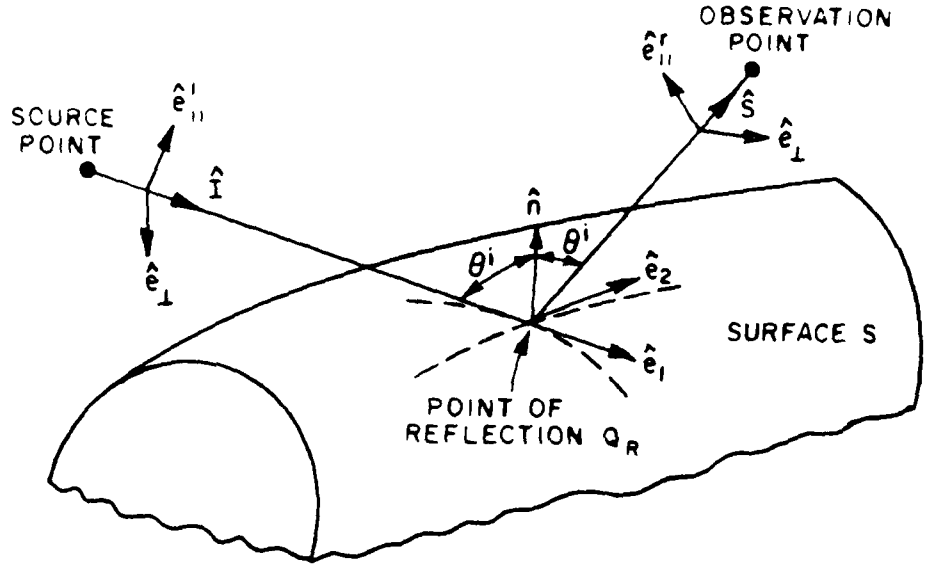

Figure 7. Reflection by a smooth convex surface.

$\bar{\bar{R}}$ is the dyadic reflection coefficient expressed as

$$\bar{\bar{R}} = \hat{e}^i\hat{e}^r - \hat{e}^i\hat{e}^r \tag{24}$$

The unit vectors $e^r_{\parallel}$ and $e^i_{\parallel}$ are parallel to the plane of incidence and the unit vectors $e^i_{\perp}$, $e^r_{\perp}$ are perpendicular to the plane of incidence. The reflection point Q_r must be determined from the law of reflection

$$-\hat{I} \cdot \hat{n} = \hat{s} \cdot \hat{n} \tag{25}$$

and

$$\hat{I} \times \hat{n} = \hat{s} \times \hat{n} \tag{26}$$

or simply stated, (25) states that the angle of incidence is equal to the angle of reflection, and (26) states that the incident, reflected and surface normal vector all lie in the same plane. The quantities $\rho_1\rho_2$ are the principal radii of curvature of the reflected wave. These were given by Kouyoumjian and Pathak [4] for spherical wavefronts as

$$\frac{1}{\rho_{1,2}} = \frac{1}{s'} + \frac{1}{\cos\theta^i}\left[\frac{\sin^2\theta_2}{R_1} + \frac{\sin^2\theta_1}{R_2}\right] \pm \sqrt{\left[\frac{1}{\cos^2\theta^i} + \frac{\sin^2\theta_2}{R_1} + \frac{\sin^2\theta_1}{R_2}\right]^2 - \frac{4}{R_1R_2}} \tag{27}$$

where s' is the distance from the source to Q_r, θ is the angle between the direction of the incident ray I and unit vector $\hat{e}$, and θ_2 is the angle between incident ray I and unit vecotr e_2.

B. Curved Surface Diffraction and UTD

The geometrical optics field is valid only when the source and observation points are not hidden by the structure and the observation point is well away from the shadow boundary. A more general case is when the observation point can be anywhere in the space around the structure. This problem is much more complex. Although the results given in this section are valid for any convex surface we will limit our discussion to an elliptical cylinder which is infinite in extent. This will serve to demonstrate the essential points of the solution without adding unnecessary complication. The regions of interest around an elliptic cylinder are shown in Figure 8. The uniform GTD (UTD) ansatz of Pathak et al. [3] was chosen because of its good continuity through the shadow boundary where previous theories failed. This solution is valid when the source and/or observation points are in regions I, II, and III.

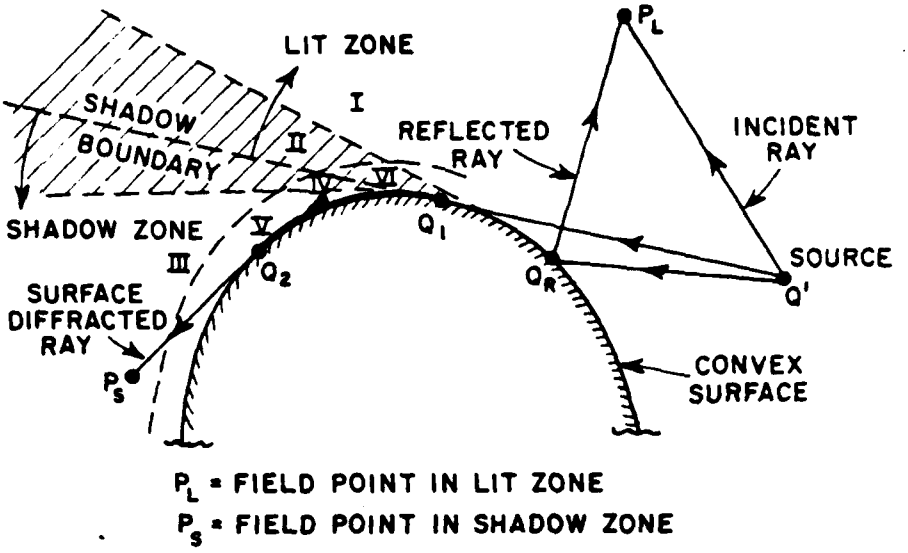

Figure 8. The rays and regions associated with scattering by a smooth convex cylinder.

The geometries to be considered are shown in Figures 7 and 9. Figure 7 shows the geometry to be considered when the observation point is in the lit zone (reflection). Figure 9 shows the geometry to be considered when the observation point is in the shadow region (creeping wave diffraction). Note that for this case the ray couples to the surface at point Q_1 and then "creeps" along the curved surface to the shed point Q_2. For the reflection problem the scattered field is computed as in the geometrical optics case but with a generalized $\bar{R}$ dyadic. In the creeping wave problem, the scattered field is computed from the incident field and the F dyadic. Referring to the appropriate geometry, the $\bar{R}$ and $\bar{T}$ dyadics are defined as

$$\bar{R} = R_s \hat{e}_\perp^i \hat{e}_\perp^r + R_h \hat{e}_{\parallel}^i \hat{e}_{\parallel}^r \tag{28}$$

$$\bar{T} = T_s \hat{\theta}_1 \hat{\theta}_2 + T_h \hat{n}_1 \hat{n}_2 \tag{29}$$

where

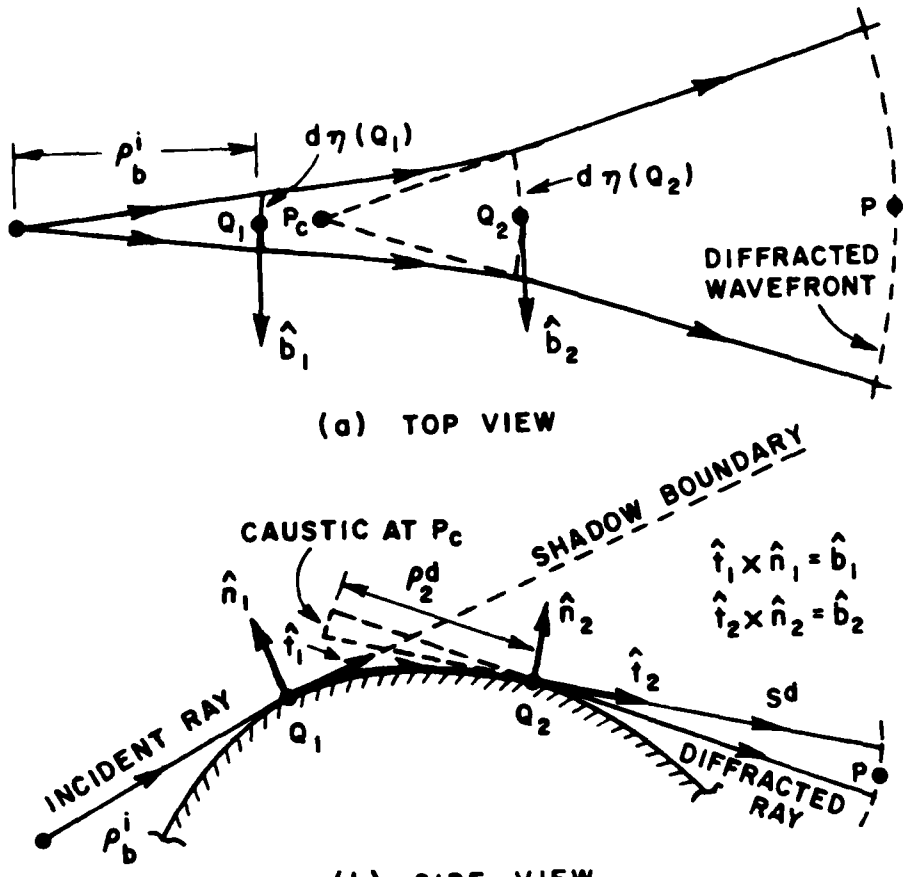

Figure 9. Diffraction by a smooth curved surface.

$$R_{\substack{s \\ h}} = -\left[\sqrt{\frac{-4}{L}}\, e^{-j(\xi^L)^3/12}\, \frac{e^{-j\frac{\pi}{4}}}{2\sqrt{\pi}\xi^L} \left\{\left[1-F(X^L)\right] + \hat{p}_{\substack{s \\ h}}(\xi^L)\right\}\right], \text{ for the } \underline{\text{lit}} \text{ region} \tag{30}$$

and

$$T_{\substack{s \\ h}} = -\left[\sqrt{m(Q_1(m(Q_2)}\, \sqrt{\frac{2}{k}}\, \frac{e^{-j\frac{\pi}{4}}}{2\sqrt{\pi}\xi^d} \left\{\left[1-F(X^d)\right] + \hat{p}_{\substack{s \\ h}}(\xi^d)\right\}\right] \sqrt{\frac{d\eta(Q_1)}{d\eta(Q_2)}}\, e^{-jkt},$$

for the
<u>shadow</u> region. (31)

with

$$\xi^L = -2m(Q_R)\, f(Q_R)^{-1/3} \cos\theta^i ; \qquad f(Q_R) = 1 + \frac{\rho_g(Q_R)}{\rho_t(Q_R)} \cos^2\theta^i ; \quad \xi^d = \int_{Q_1}^{Q_2} dt' \, \frac{m(t')}{g(t')} ; \tag{32a,b,c}$$

$$m(Q) = \left[\frac{k\rho_g(Q)}{2}\right]^{1/3} ; \qquad t = \int_{Q_1}^{Q_2} dt' ; \tag{32d,e}$$

$$\chi^L = 2k L^L \cos^2\theta^i ; \qquad \chi^d = \frac{k\, L^d (\xi^d)^2}{2m(Q_1)m(Q_2)} . \tag{32f,g}$$

Thus with the $\overline{\overline{R}}$ and $\overline{\overline{T}}$ dyadics computed, the scattered fields can be computed by

$$E(P_L) \sim \overline{E}^i(P_L) + \overline{E}^i(Q_R) \cdot \overline{\overline{R}} \sqrt{\frac{\rho_1^r \rho_2^r}{(\rho_1^r + s^r)(\rho_2^r + s^r)}}\, e^{-jks^r} ; \quad \text{for } P_L \text{ in the } \underline{\text{lit}} \text{ region} \tag{33}$$

$$\overline{E}(P_s) \sim \overline{E}^i(Q_1) \cdot \overline{\overline{T}} \sqrt{\frac{\rho_2^d}{s^d(\rho_2^d + s^d)}}\, e^{-jks^d} ; \quad \text{for } P_s \text{ in the } \underline{\text{shadow}} \text{ region} \tag{34}$$

Note that in the above equation

$$[1 - F(\sigma)] \to 0 \text{ in the region exterior to zone II}$$

$$\hat{P}_{\substack{s \\ h}}(\delta) \sim \pm \left\{ \begin{matrix} R_s \\ h \end{matrix} \right\} \sqrt{\frac{-\delta}{e}}\, e^{j\frac{\delta^3}{12}} \quad \text{in zone I} . \tag{35}$$

Thus the above solution reduces to the geometrical optics solution in the visible region away from the shadow boundary (zone I).

The parameters L^L and L^d are distance parameters relating to the relative sizes of s,s'. for a spherical wave they are given by

$$L^L = \frac{ss'}{s+s'}$$

$$L^d = \frac{ss'}{s+s'}$$

While Equations (33) and (34) are valid and continuous at the shadow boundary they are only true in the limit since the parameters ξ^L and ξ^d are both zero on the shadow boundary. A limit form of the solution which can be employed in this region is

$$\begin{pmatrix}\hat{b}_1\\ \hat{n}_1\end{pmatrix}\cdot\bar{E}^i(P_{SB}) - \begin{pmatrix}\hat{b}_1\\ \hat{n}_1\end{pmatrix}\cdot\bar{E}^i(Q_1)\left[\frac{\sqrt{L^L}}{2} + m(Q_1)\ \frac{2}{k}\,e^{j\frac{\pi}{4}}\begin{pmatrix}p^*(0)\\ q^*(0)\end{pmatrix}\sqrt{\frac{1}{2}\left(\frac{\rho_2^r}{\rho_2^r+s}\right)}\right]e^{jks}$$

$$= \begin{pmatrix}\hat{b}_1\\ \hat{n}_1\end{pmatrix}\cdot\bar{E}^i(Q_1)\left[-\frac{\sqrt{L^d}}{2} + m(Q_1)\ \frac{2}{k}\,e^{j\frac{\pi}{4}}\begin{pmatrix}p^*(0)\\ q^*(0)\end{pmatrix}\sqrt{\frac{1}{2}\left(\frac{\rho_2^d}{\rho_2^d+s}\right)}\right]e^{-jks}, \tag{36}$$

The $\hat{P}_{s_h}(\xi)$ functions of Equations (30,31) are defined in terms of the related functions $p^*(\xi)$ and $q^*(\xi)$ by

$$\hat{P}_{s_h}(\delta) = \begin{Bmatrix}p^*(\delta)\\ q^*(\delta)\end{Bmatrix} e^{-j\frac{\pi}{4}} - \frac{e^{-j\frac{\pi}{4}}}{2\delta\sqrt{\pi}} \tag{37}$$

where the $p(\delta)$ and $q(\delta)$ functions, defined by Logan [6] are plotted in Figures 10a,b over the region $-3<\sigma<2$. More complete descriptions of these functions are given in [2] and [5]. The transition function $F(\delta)$ which also appears in formulas (30), (31) is defined [4] in terms of the Fresnel integral as

$$F(\delta) = 2j\ \delta\ e^{jx}\int_{|\sqrt{\sigma}|}^{\infty} e^{-j\tau^2}\,d\tau\ . \tag{38}$$

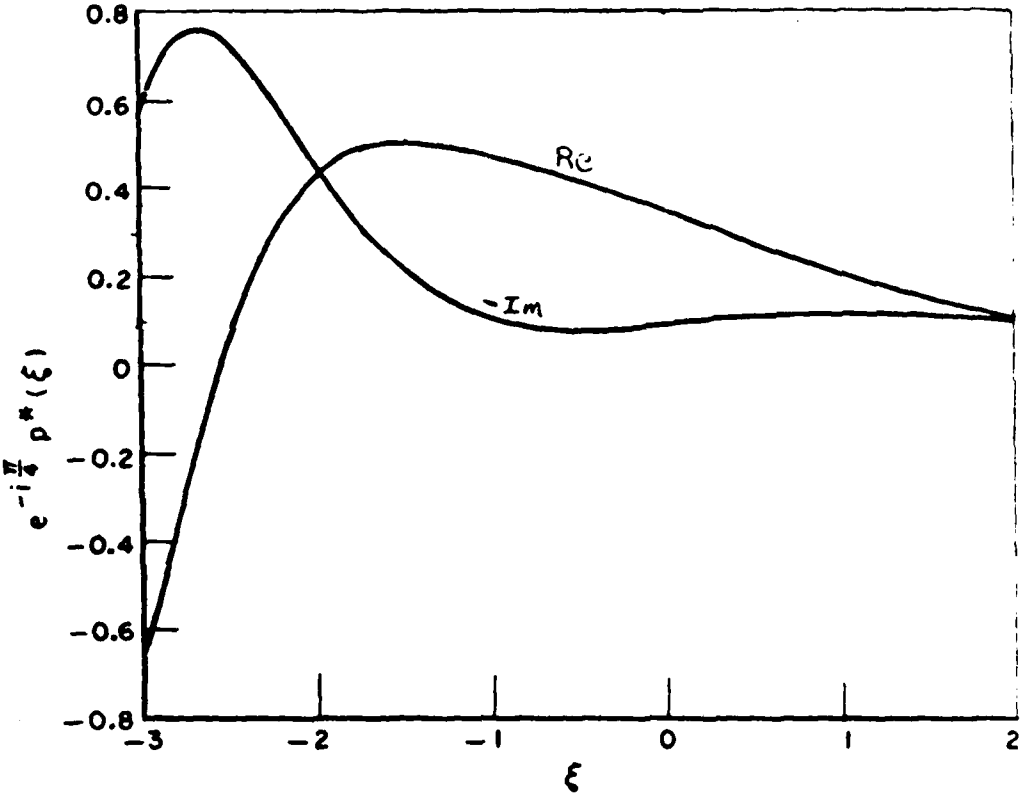

Figure 10a. Plot of $e^{-j\pi/4}\ p^*(\xi)$ vs ξ based on Logan's tabulated data [6] for $p(\xi)$.

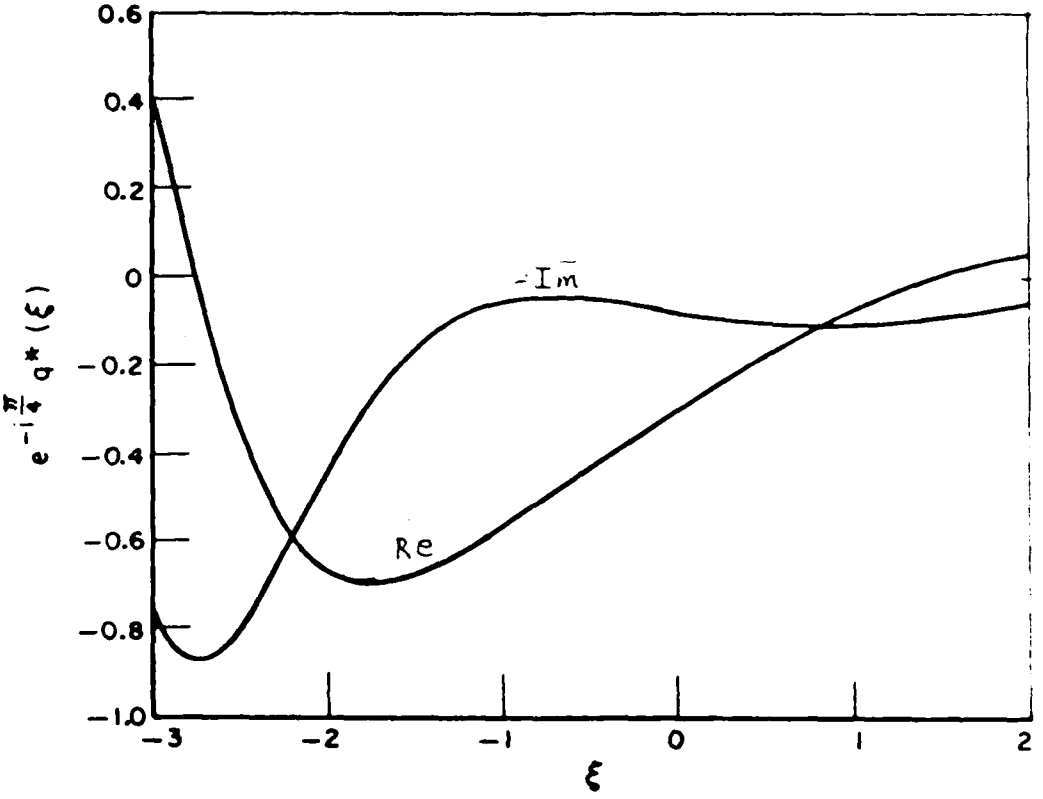

Figure 10b. Plot of $e^{-j\pi/4} q^*(\xi)$ vs ξ based on Logan's tabulated data [6] for $q(\xi)$.

CHAPTER IV
THE HYBRID METHOD

The hybrid method to be presented here is a technique for analyzing thin wire antennas which are not electrically large in the presence of a body or scatterer which is too large to be handled by the moment method. This is accomplished by computing a second moment method impedance matrix proposed by Thiele et al [7]. This second matrix $[\Delta Z]$ is a perturbation to the original $[Z]$ and includes the coupling between the test and expansion modes due to rays reflected and diffracted from the nearby structure.

Using the GTD ray optics technique, the electric field incident on a wire scatterer due to radiation from another wire scatterer, can be written as

$$E_s^i = E_s^o + E_s^i + E_s^2 \cdots E_n^n \tag{39}$$

where E_s^o is the incident field due to the direct path (free space case) and $E_s^1 \cdots E_s^n$ denote the fields due to the various rays which are reflected or diffracted by the nearby body. Note that for the case where the body hides the source from the observer then $E_s^o = 0$. Using Equation (39) the component Z_{mn} of the $[Z]$ matrix can be written

$$Z_{mn} = \int [E_s^o(\ell) + E_s^1(\ell) + E_s^2 \cdots E_s^n] \cdot I(\ell) d\bar{\ell} \tag{40}$$

which can be written as

$$Z_{mn} = Z'_{mn} + \Delta Z_{mn} \tag{41}$$

where

$$Z'_{mn} = \int E_s^o(\ell) \cdot I(\ell) d\bar{\ell} \tag{42}$$

and

$$\Delta Z_{mn} = \int (E_s^1(\ell) + E_s^2(\ell) \cdots E_s^n(\ell) \cdot I(\ell) d\bar{\ell} \tag{43}$$

and thus in matrix form

$$[Z] = [Z'] + [\Delta Z] \tag{44}$$

Where $[Z']$ is computed using the direct (free space) path between source and observation point and $[\Delta Z]$ is computed using the ray paths which interact with the large body. Thus the effect of the large body are included in the moment formulation and the solution obtained will therefore contain these interactions. One problem which arises from Equation (39) is that the GTD requires that the field generated by the sources contain no ray path components. In general this condition cannot be met. Fortunately, the PWS expansion function used by Richmond can be shown to have only transverse field components as follows;

Eckelman [1] observed that the fields of a piecewise sinusoidal test dipole can be broken up into contributions from the endpoints and the driving points. These fields have spherical wavefronts and thus are in the required form for using them as sources with the GTD (UTD). With reference to Figure 5, the exact field of a PWS dipole is

$$E_1 = \frac{-j\eta I_o}{4\pi \sin(kd)} \frac{e^{-jkR_1}}{R_1} \frac{1}{\sin\theta_1} \tag{45a}$$

$$E_2 = \frac{j\eta I_o 2\cos(kd)}{2\pi \sin(kd)\sin\theta_2} \frac{e^{-jkR_2}}{R_2} \tag{45b}$$

$$E_3 = \frac{-j\eta I_o}{4\pi \sin(kd)} \frac{e^{-jkR_3}}{R_3} \frac{1}{\sin\theta_3} \tag{45c}$$

Thus using the above result, the coupling between a test source and an expansion mode proceeds as follows:

A term Z_{mp} of the Z matrix is computed in the standard form using formula (20), this gives the coupling due to the direct ray path. Note that if the test and expansion modes are hidden by the cylinder then this Z_{mp} will be zero. The elements of ΔZ_{mp} are computed also using formula (20) where E^s_θ is the field scattered from the cylinder. This includes all significant fields from all ray paths of interest. For this paper, these ray paths are defined by the statements:

i) if the observation point is not shadowed, only the reflected field is included.

ii) if the observation point is shadowed the rays corresponding to creeping around the cylinders in a clockwise and a counter-clockwise sense.

These are the significant terms for an infinite cylinder. If the cylinder were not infinite, scattering from the end caps would have to be included.

The total impedance matrix is then computed as

$$[Z] = [Z'] + [\Delta Z]$$

Once the [V] matrix has been computed (in the usual manner), then [I] can be found by matrix inversion or any other suitable technique. Once again, it is important to note the significance of using Richmond's piecewise sinusoidal test function for the test sources. As a result of the endpoint separation technique of Eckelman each term in $[\Delta Z]$ can be computed by integrating only over the expansion mode, and using the field radiated by the endpoints of the test function. For a general test function, two problems would arise which would greatly reduce the numerical efficiency and accuracy of the process.

1) The expression for the coupling would contain a double integral: one over the source, to compute the incident field at a point on the observer, and one over the observer to compute the actual coupling.

2) The fields radiated by the source would not necessarily be transverse to the direction of propagation, which cannot be handled using GTD.

CHAPTER V
DIPOLES NEAR AN ELLIPTIC CYLINDER

The first application of the theory presented in Chapters II, III, and IV is the analysis of dipoles near an infinite, perfectly conducting, elliptic cylinder. The elliptic cylinder was chosen because it has found wide application in the past. It can be used to model aircraft fuselages and engines as well as antenna masts on ships and land based systems.

The dipole is of prime interest because as shown in the earlier chapter on the moment method, the [Z] matrix can be obtained by computing the coupling between the mth test function and the nth expansion mode. In the case of Richmond's thin wire code, these modes are dipoles with a piecewise sinusoidal current distribution. Thus once one can calculate the near field coupling between dipoles near an object, any thin wire antenna near the object can be analyzed.

A. Overview

The geometry to be considered consists of two piecewise sinusoidal dipoles located in the vicinity of an infinite, perfectly conducting elliptic cylinder which is aligned with the $\hat{z}$ axis. One dipole will be referred to as the source; the other dipole will be called the observer. These designations are arbitrary since by reciprocity the source and observers can be interchanged without affecting the coupling. Coupling will be computed using Equation (20). The integration over the observer will be carried out numerically by dividing the observer up into subsection and using Simpson's rule integration. The fields radiated by the source will be spherical waves eminating from the driving point and the two endpoints. For rays which interact with the cylinder, the diffraction or reflection coefficients will be computed using the UTD presented in Chapter III. Examination of the UTD expressions shows that it is first necessary to determine whether or not the cylinder hides the source from the observer.

B. Location of Observer

The question of determining whether the cylinder hides the source can be resolved by determining whether or not a direct ray from source to observer will intersect the cylinder. Since the cylinder is infinite in length, the geometry can be reduced to a two

dimensional problem in the x, y plane. Consider the geometry shown in Figure 11. The equation of the line $(x_s y_s)(x_c y_c)$ can be written as

$$y = mx + c \tag{46}$$

where

$$m = \frac{y_s - y_r}{x_s - x_r} \quad \text{and} \quad c = y_s - mx_s \tag{47a,b}$$

the equation for an ellipse is

$$\frac{x^2}{a^2} + \frac{y^2}{b^2} = 1 \tag{48}$$

thus Equations (46), (47a,b) and (48) can be combined to give

$$m^2 + \frac{b^2}{a^2} \quad x^2 + 2mcx + (c^2 - b^2) = 0 \tag{49}$$

then using the quadratic formula

$$x_{1,2} = \frac{-2mc \pm \sqrt{4\, m^2c^2 - 4\left(m^2 + \frac{b^2}{a^2}\right)(c^2 - b^2)}}{2\left(m^2 + \frac{b^2}{a^2}\right)} \tag{50}$$

If $x_{1,2}$ are complex conjugates, then no solution exists in the x,y plane, and thus the line does not intersect the cylinder at all. If $x_{1,2}$ exist then the situation shown in Figure 12 can be detected as follows: If $x_c < x_{1,2} < x_s$ or $x_s < x_{1,2} < x_c$ then the source is hidden, otherwise a condition like Figure 12 exists and the source is obviously not hidden.

C. Spectral Point Calculation

If the wave is not hidden, then it is necessary to find the reflection point. Marhefka[2] outlined a procedure for finding the reflection point on an elliptic cylinder assuming the source point and the scatter direction were known. Ekelman modified this procedure for the case where the source point and observation point were known. This procedure, while accurate, is inefficient. The solution presented here works well for a large class of problems

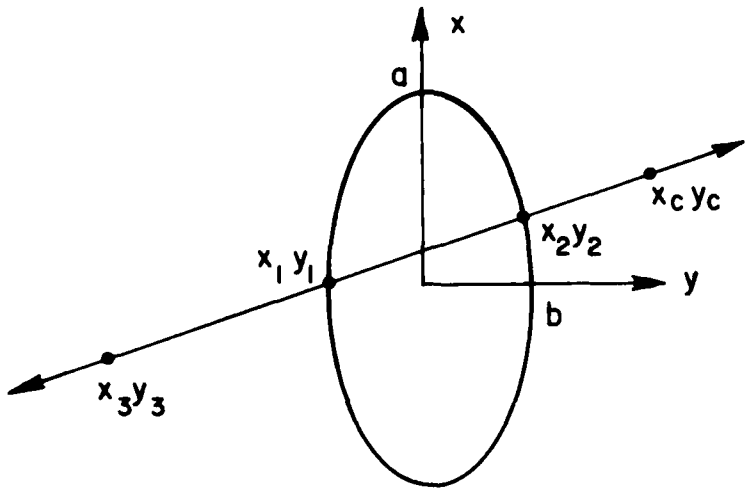

Figure 11. Geometry for determining whether or not the source $(x_s y_x)$ is hidden by the cylinder.

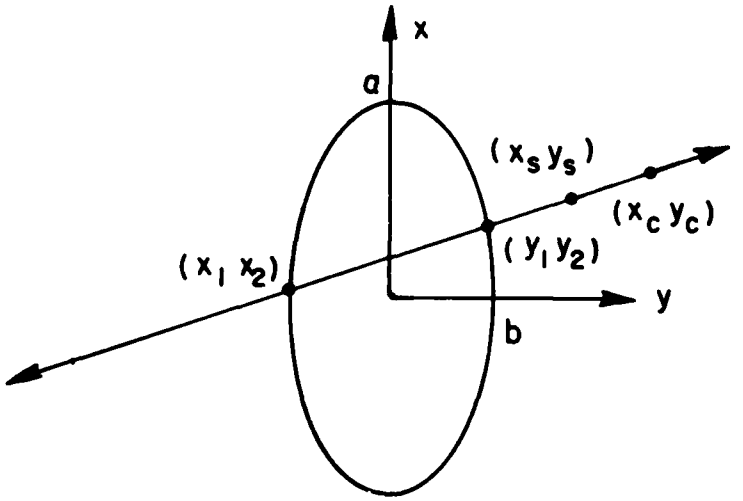

Figure 12. Line $(x_s y_s)$ $(x_c y_c)$ intersects the cylinder but source is not hidden.

when neither the source nor observation point are in the far field of the cylinder.

The geometry of the problem is shown in Figure 13. The source and observation points are in the vicinity of an elliptic cylinder and the reflection point $(x_r y_r z_r)$ on the surface of the cylinder is desired, and it is assumed that the cylinder does not hide the source from the observation point. Marhefka [2] formulates the problem using the laws of reflection and shows that the problem can be decomposed into a two dimensional problem in x and y, and a one dimensional problem in z.

Consider the two dimensional problems shown in Figure 14. The incident and observation vectors can be written

$$\bar{I}(v,z) = I_x(v)\hat{x} + I_y(v)\hat{y} + I_z(z)\hat{z}$$

$$= (a\cos v - x_s)\hat{x} + (b\sin v - y_s)\hat{y} + (z - z_s)\hat{z} \qquad (51)$$

and

$$\bar{d}(v,z) = d_x(v)\hat{x} + d_y(v)\hat{y} + d_z(z)\hat{z}$$

$$= (x_c - a\cos v)\hat{x} + (y_c - b\sin v)\hat{y} + (z_c - z)\hat{z} \quad . \qquad (52)$$

Using Fermat's Principle, the reflection point will be determined by that v which minimizes s(v)

$$s(v) = |I(v)| + |d(v)| \qquad (53)$$

where

$$|I(v)| = [(a\cos v - x_s)^2 + (b\sin v - y_s)^2]^{1/2} \qquad (54)$$

$$|d(v)| = [(x_c - a\cos v)^2 + (y_c - b\sin v)^2]^{1/2} \quad . \qquad (55)$$

The extrema of s(v) can be found by computing the roots of s'(v). Since s(v) is a non-linear function it will be necessary to use a numerical procedure, and Newton's method will work well here. Substituting

$$\alpha = \cos v \qquad (56a,b)$$
$$\beta = \sin v$$

and

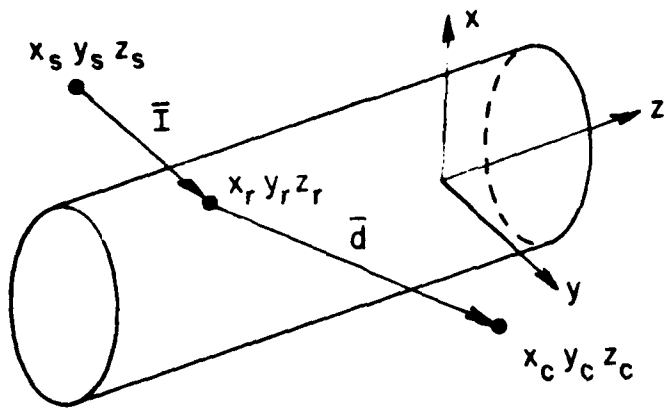

Figure 13. Three dimensional geometry for determining reflection point.

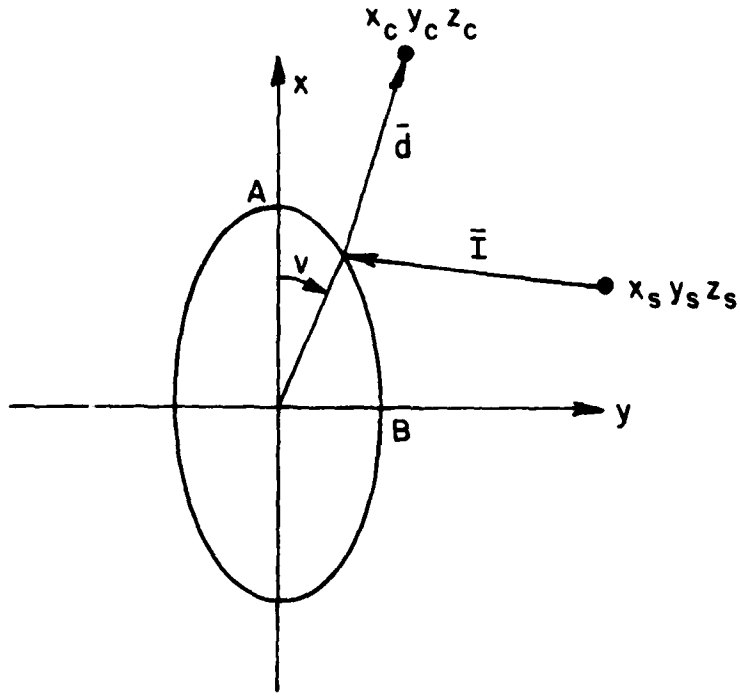

Figure 14. Two dimensional geometry for determining reflection point in x,y plane.

$$h(v) = (a\alpha - x_c)^2 + (b\beta - y_c)^2 \tag{57}$$

$$g(v) = (a\alpha - x_s)^2 + (b\beta - y_s)^2 \tag{58}$$

then

$$s(v) = \sqrt{h} + \sqrt{g} \tag{59}$$

and

$$s'(v) = \frac{\sqrt{g}\, h' + \sqrt{h}\, g'}{2\, hg} \tag{60}$$

$$s''(v) = \frac{[2h''h(h')^2]g^{3/2} + [2g''g - (g')^2]h^{3/2}}{4(hg)^{3/2}} \tag{61}$$

Now using Newton's method

$$v_{n+1} = v_n - \frac{s'(v)}{s''(v)}$$

by observation of the physical problem it is apparent that $s'(v)$ will have at most four and at least two roots. The four root case (two maximums and two minimums) occurs when the source and observation points are near enough so that the path through the cylinder is shorter than the path to the ends (Figure 15). In any case the second minimum will always lie outside the visible region.

Newton's method requires that an initial value of v be found to start the iteration process. If the initial value is close to the desired result then successive iterations will always converge to the desired root and the other roots need not be calculated. No method has been determined to pick such an initial value. The other alternative is to choose a result which is known to converge to the desired root most of the time. The value then obtained is checked to insure that the true reflection point has been determined; if not, then a slower but more reliable method can be employed, or a new initial value can be chosen based on some different criterion.

Numerical analysis has shown that the value of v_1 given in Equation (63) will converge to the proper root in almost all cases. A wide variety of cylinder source and observation points were tested and this criterion was found to fail only for a certain orientation when $\frac{A}{B} >> 1$ or when one point was in the far field

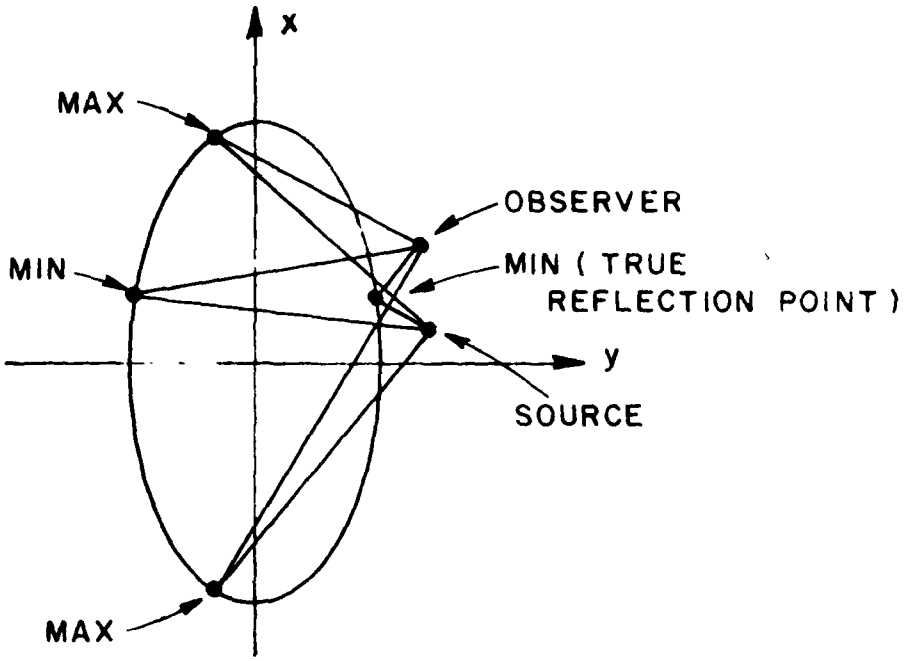

Figure 15. Various examples of the extremia for the source, cylinder, observer ray path.

$$v_s = \tan^{-1}\left(\frac{ay_s}{bx_s}\right) \tag{62a}$$

$$v_c = \tan^{-1}\left(\frac{ay_c}{bx_d}\right) \tag{62b}$$

$$v_1 = \begin{cases} \dfrac{v_s+v_c}{2} & |v_s+v_c| > \pi \quad (63a) \\ \dfrac{v_s+v_c}{2} + \pi & |v_s+v_c| > \pi \quad (63b) \end{cases}$$

Once a root has been found using v_1 it is necessary to determine if it is the true reflection point. There are two possibilities for error: 1) it has converged to a maximum, 2) it has converged to a minimum not in the visible region. For the first case it is necessary only to check $s''(v)>0$. In the second case, it is necessary to determine whether the lines $(x_s y_s)$ to $(x_r y_r)$ or $(x_c y_c)$ to $(x_r y_r)$

intersect the cylinder (except at the point $(x_r y_r)$. Since

$$x_r = A \cos v \tag{64}$$

and

$$y_r = B \sin v \tag{65}$$

then from formula (49)

$$(m^2 + \frac{b^2}{a^2})\, x^2 + 2mcx + (c^2 - b^2) = 0 \tag{66}$$

Since one root of the equation is already known to be $x_1 = x_r$, then by division the second root is

$$x_2 = - \frac{2mc - x_r(m^2 + \frac{b^2}{a^2})}{m^2 + \frac{b^2}{a^2}} \tag{67}$$

The intersection points have now been calculated and it is a simple matter to test whether or not the ray path intersects the cylinder testing whether $x_r < x_2 < x_s$ or $x_r > x_2 > x_s$.

D. Tangent Points

For the case where the source is hidden by the cylinder, the reflection point does not exist. In that case it is necessary to compute the tangent points on the cylinder since that is where the creeping waves will couple on and shed from the surface. These points (x,y) are given by [2]

$$x_t^{12} = \frac{a^2 b^2 x_s \mp z^2 y_s \sqrt{a^2 y_s^2 + b^2 s_x^2 - a^2 b^2}}{(a^2 Y_s^2 + b^2 x_x^2)} \tag{68}$$

$$y_t^{1,?} = \frac{a^2 b^2 y_s \pm b^2 x_s \sqrt{a^2 y_s^2 + b^2 x_3^2 - a^2 b^2}}{(a^2 y_s^2 + b^2 y_s^2)} \tag{69}$$

the tangent angles can then be found from

$$v_{i_{1,2}} = \tan^{-1}\left(\frac{ay_t^{1,2}}{bx_t^{1,2}}\right) \tag{70}$$

once the tangent points are known in the (x,y) plane, the clockwise and counter clockwise paths around the cylinder can quickly be determined. The only unknowns at this point are the $\hat{z}$ coordinates of the coupling points. The $\hat{z}$ coordinate can be determined by making use of the fact that the elliptic cylinder is a developed surface.

$$= z_{c_s} \pm d_{os}\,\frac{(z_c - z_s)}{(d_{os}+t+d_{oc})} \tag{71}$$

where

$$d_{os} = \sqrt{(x_s - x_{i_1})^2 + (y_x - y_{i_1})^2} \tag{72a}$$

$$d_{oc} = \sqrt{(x_c - x_{i_2})^2 + (y_c - y_{i_2})^2} \tag{72b}$$

$$t = \int_{Q_1}^{Q_2} \sqrt{a^2\sin^2(v) + b^2\cos^2(v)}\; dv \tag{73}$$

E. Results

Figures 17, 18 show plots of the coupling between two $\lambda/2$ dipoles using the geometry given in Figure 16. The data is plotted with the field computed by the NEC Basic Scattering Code [5,12].

The NEC is a computer program developed at the Ohio State University ElectroScience Laboratory. It computes the far field scattering of electric and magnetic sources in the vicinity of elliptic cylinders and/or finite plates. This code was chosen as a basis for comparison because of its flexibility and proven accuracy. Since the fields computed by NEC are scattered electric fields, they can be used for comparison only with the following points in mind.

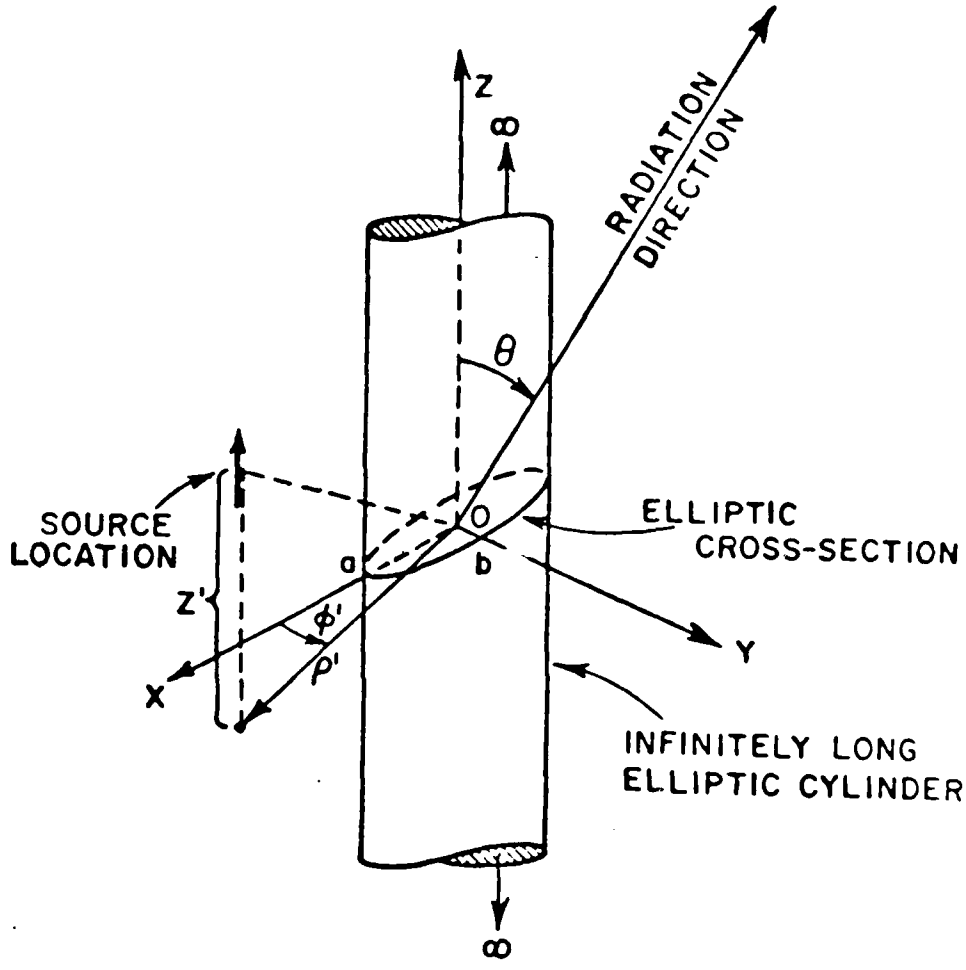

Figure 16. 3-D scattering configuration involving an infinitely long elliptic cylinder.

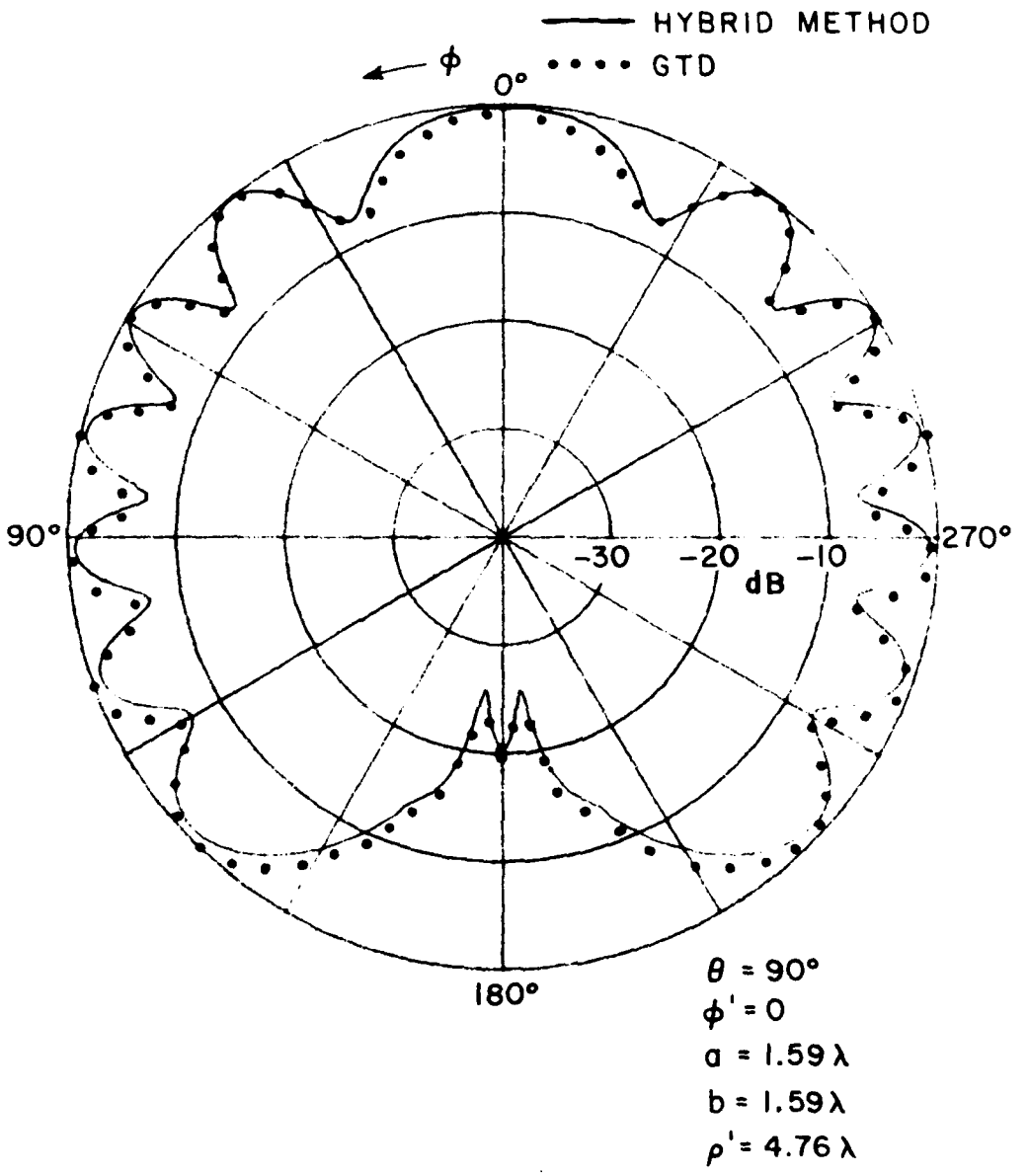

Figure 17. Comparison of coupling and E_θ radiation of an electric dipole near a circular cylinder.

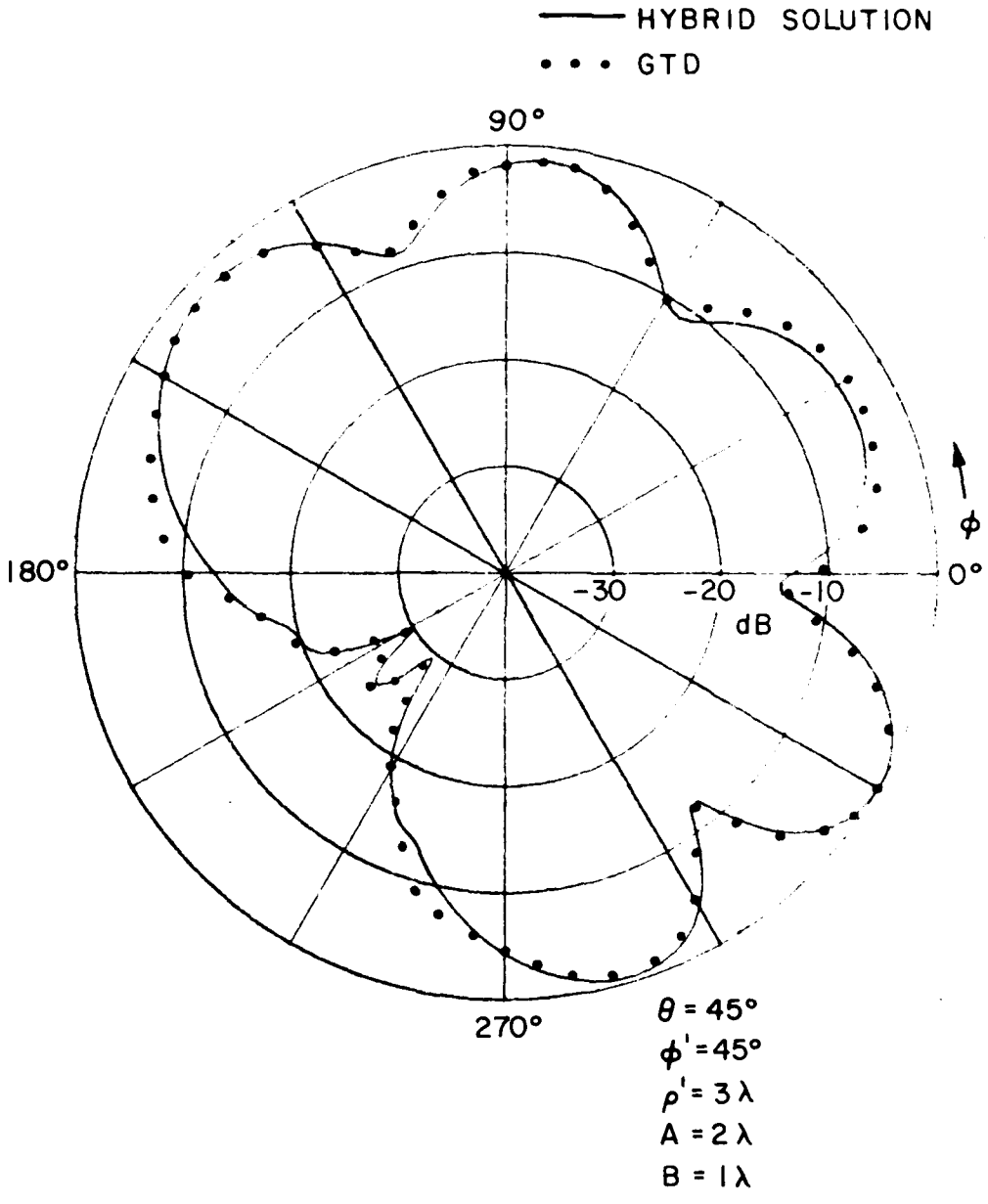

Figure 18. Far field coupling between two half-wave dipoles compared with E_θ radiation field of an axial dipole located at (ρ', ϕ').

1) The test dipole must be oriented to pick up only the components of the field computed by NEC (E_t or E_ϕ).

2) the test dipole must be far enough from the cylinder and the source dipole that the far field approximations apply.

3) Since the hybrid code is computing coupling, only the normalized pattern can be compared. This is possible because the test dipole is in the far field and short compared with its distance from the cylinder. Thus the incident field can be considered constant across its length. With a constant aggument in the integrand the incident field and coupling differ only by a constant value.

It was also desired to show that the hybrid method works well when both dipoles were near the cylinder.

A Green's function solution for the coupling between two axial PWS dipoles in the presence of an elliptic cylinder was provided by Ersoy [13]. This procedure is very similar to the hybrid technique described in this paper. A delta impedance matrix representing the cylinder effect is found via a moment method procedure. The method incorporates the cylindrical Green's function in the kernel of the integral equation. These eigenfunctions account for the presence of the cylinder. Since the eigenfunctions are in the form of a summation, accurate results are obtained when sufficient terms are included. This will be seen to pose some problems.

Figures 19 and 20 show how the hybrid and the eigenfunction solution compare using the geometry of Figure 16. Agreement is very good except in the deep shadow region. Although the eigenvalue solution is analytically exact, it could suffer from the aforementioned numerical problems. Thus another method of checking the result was desired.

F. Experimental Data

The only other method immediately available for comparison was the measurement of actual antenna systems. To avoid the problems associated with balanced and unbalanced antenna feeds, the model was constructed on a ground plane and monopoles were used instead of dipoles. Figure 21 shows the model used. A five inch diameter cylinder was mounted on the ground plane, and an aluminum "skirt" was put on the plane to reduce edge diffractions. The monopoles were constructed from 1/8" diameter brass rod and cut to 2.5" in length. The monopoles were $\lambda/4$ long at 1.1811 GHz Ekleman [1]used a similar arrangement to measure input impedance. He showed that

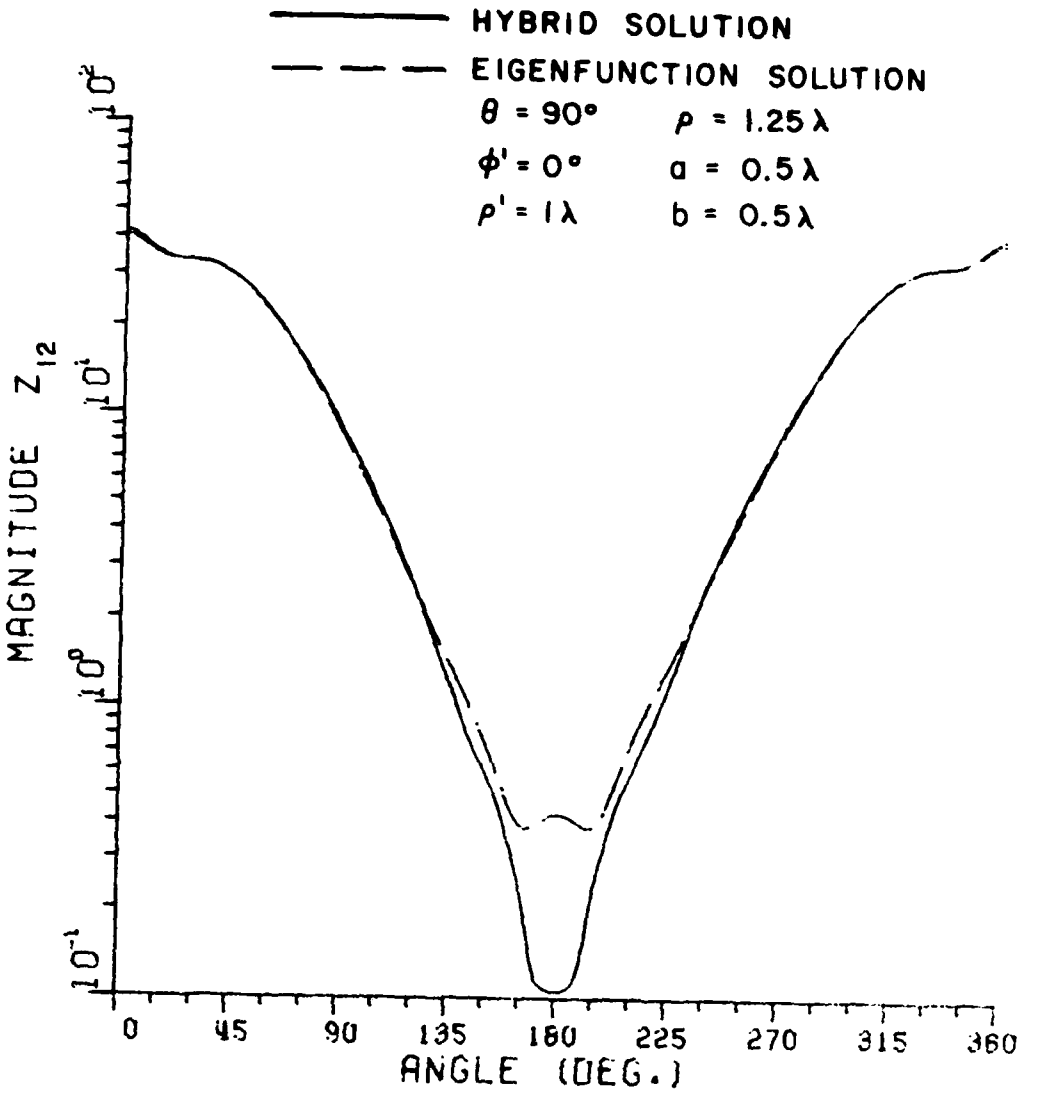

Figure 19. Magnitude of the coupling between two axial half-wave PWS dipoles near a circular cylinder.

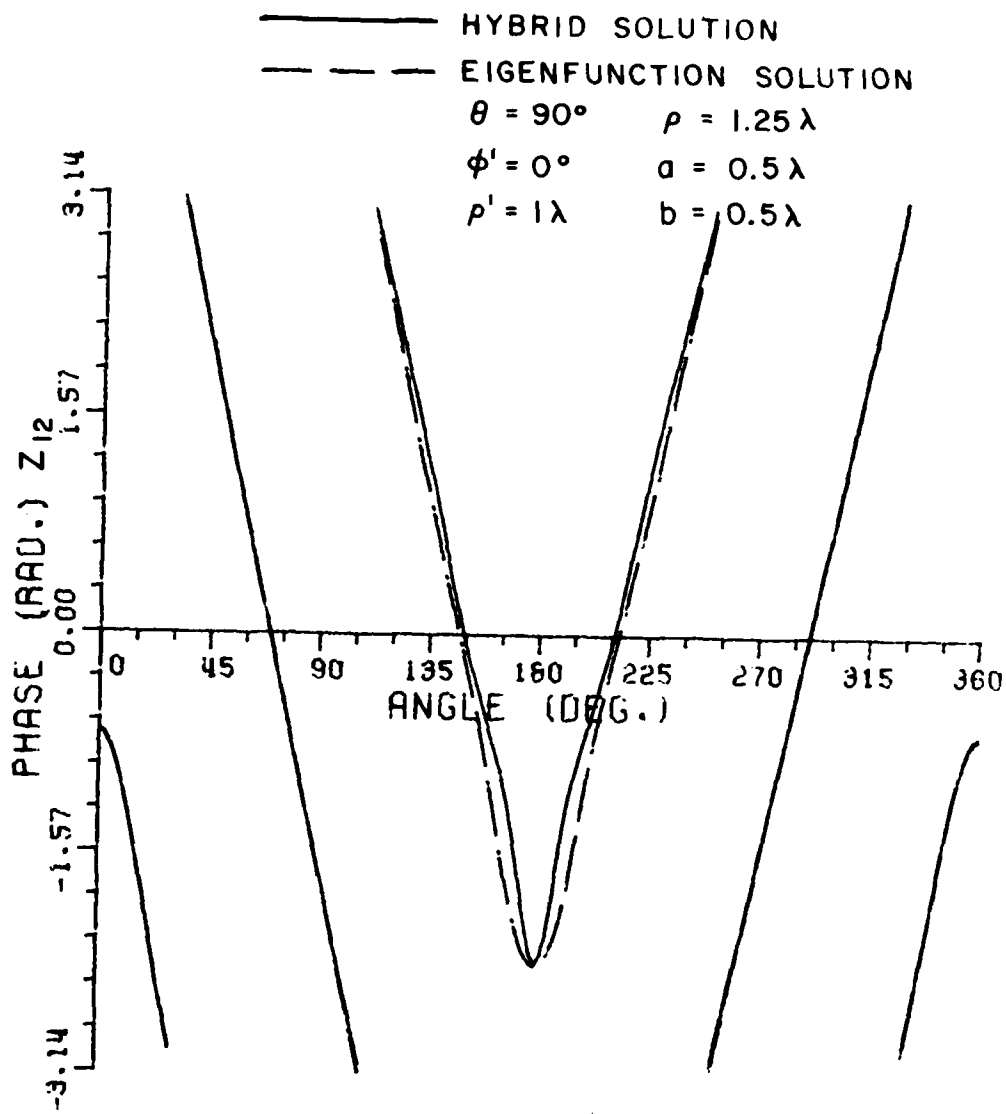

Figure 20. Phase of the coupling between two axial half-wave PWS dipoles near a circular cylinder.

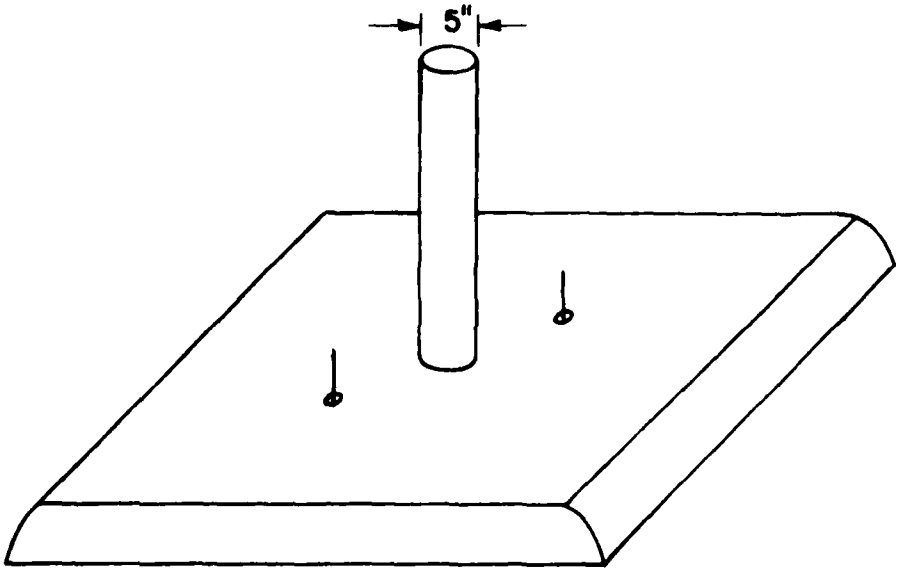

(a)

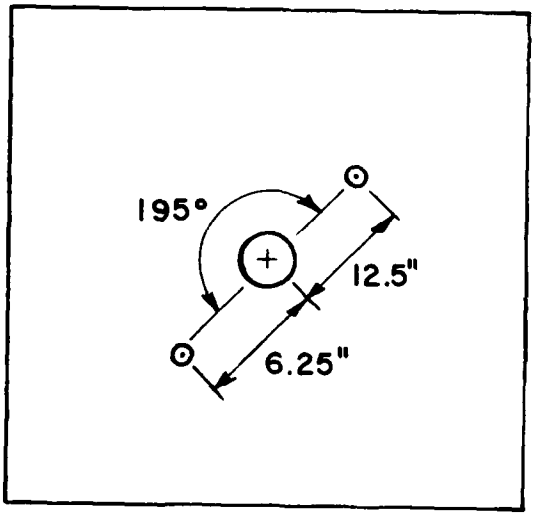

(b)

Figure 21. Geometry used in the experimental setup.

since the monopoles are moderately thick, it was necessary to lengthen the monopoles in the computational model by 1/16" to account for tip effects. This extra length was also included here.

The test equipment used was designed to accurately measure the transmission coefficient of a two port network. The two antenna system can be viewed as such a network with the input port being the terminals of the transmitting antenna and the output port being the terminals of the receiving antenna. The coupling Z_{12} is related to the transmission coefficient T_{12} by

$$T_{12} = \frac{Z_{12}}{Z_{22}} \tag{74}$$

where Z_{22} is the input impedance of the receiving antenna.

Data was taken over frequencies from 1. to 1.8 GHz. In terms of wavelengths this provided a variety of antenna lengths and cylinder sizes. The measured and computed values are shown in Figures 23 and 24. Agreement between the two sets of data is good, with the measured points showing good spread around the computed curves. Since the losses were so great($|T_{12}| \approx 44$ dB), it was necessary to use very high gain settings of the test equipment amplifier. This caused the system to be very sensitive to outside influences such as other objects in the anechoic chamber. In spite of this sensitivity, several sets of data were taken and good repeatability of the data was observed. Thus the hybrid method has been shown to accurately predict the coupling between antennas near a cylinder.

Figures 25, 26, and 27 show the coupling between various orientations of dipoles near infinite cylinders. Note that in Figure 25 the free space and diffracted curves differ only by a constant in the far field. This occurs because the path around the cylinder does not vary in that region. Note also that in Figures 25 and 26 a peak is seen in the coupling. This occurs because in the extreme near field the field is highly attenuated due to the long path around the cylinder. In Figure 27 this peak does not occur because the path around the cylinder is always getting longer.

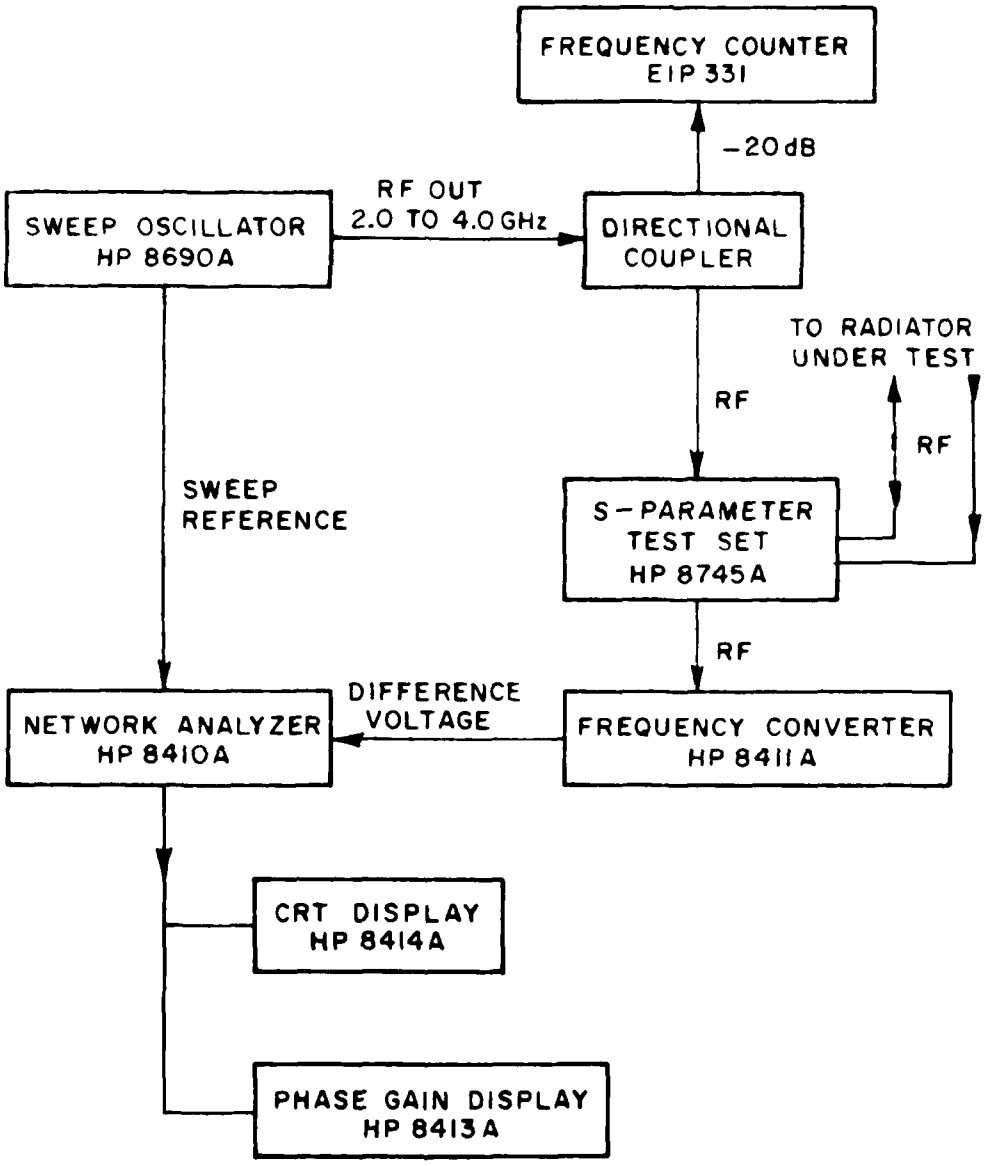

Figure 22. Block diagram of experimental measurement setup.

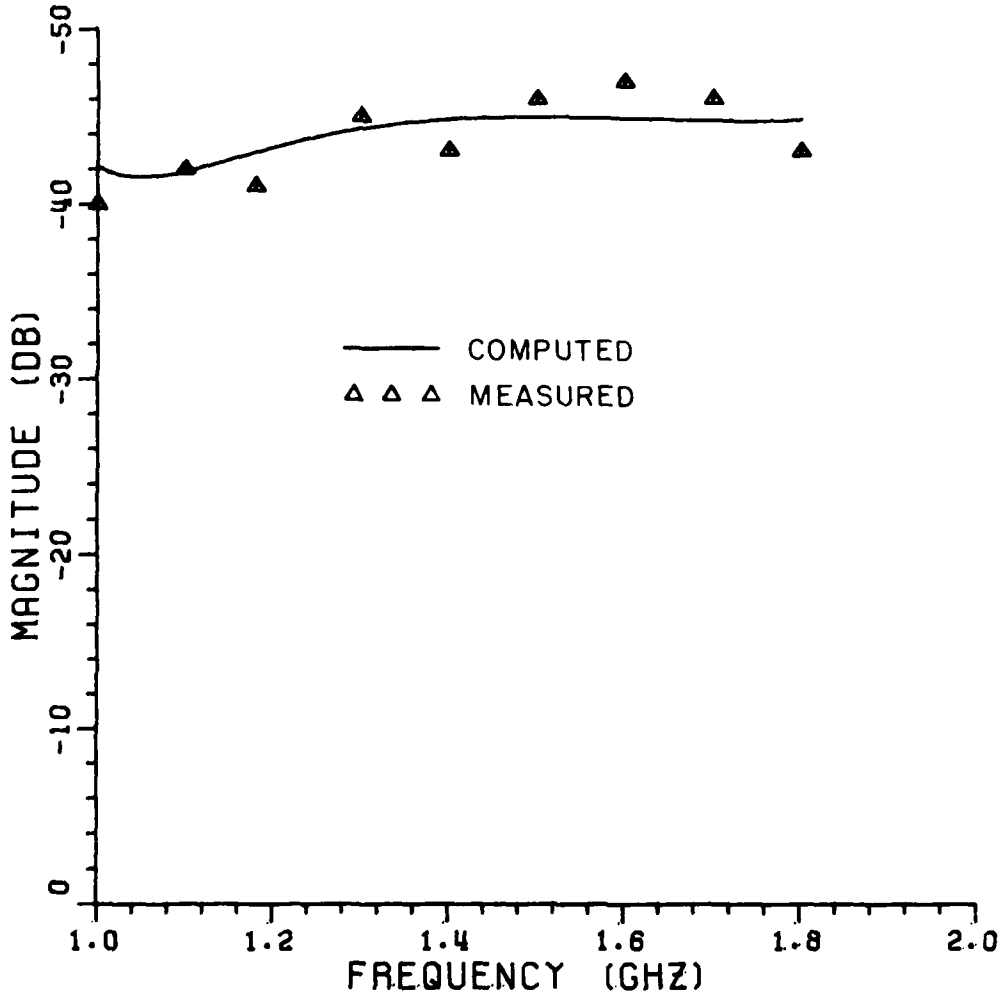

Figure 23. Magnitude of the transmission coefficient for the monopoles used in the experimental setup.

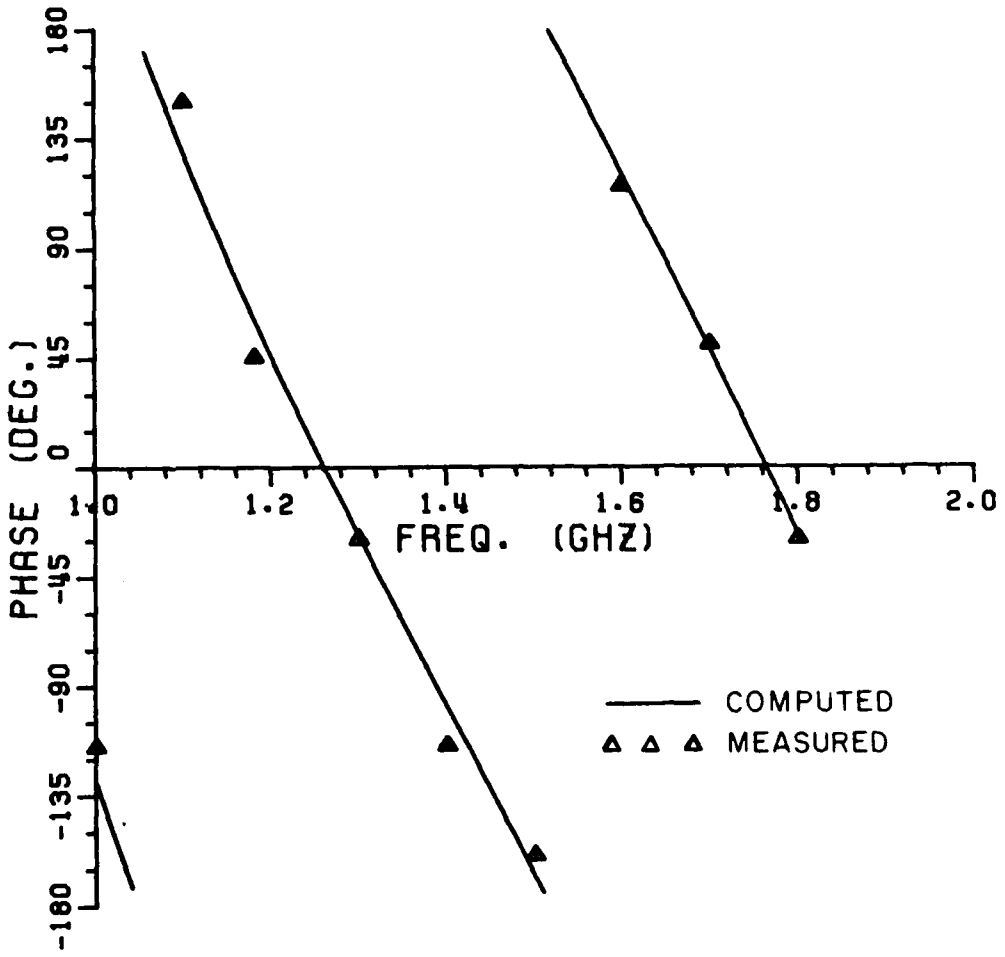

Figure 24. Phase of the transmission coefficient for the monopoles used in the experimental setup.

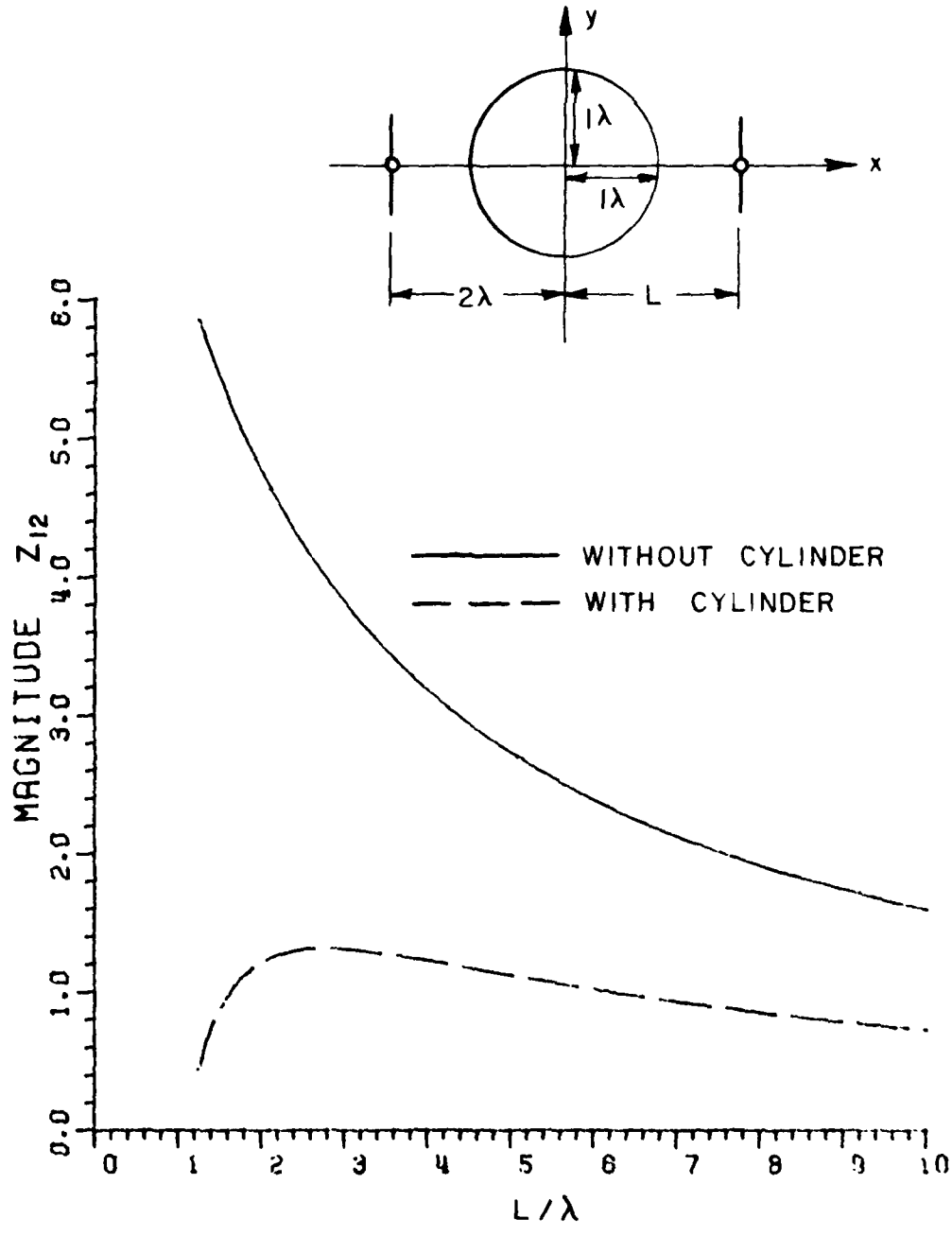

Figure 25. Comparison between free space and diffracted coupling between two PWS dipoles in the deep shadow region.

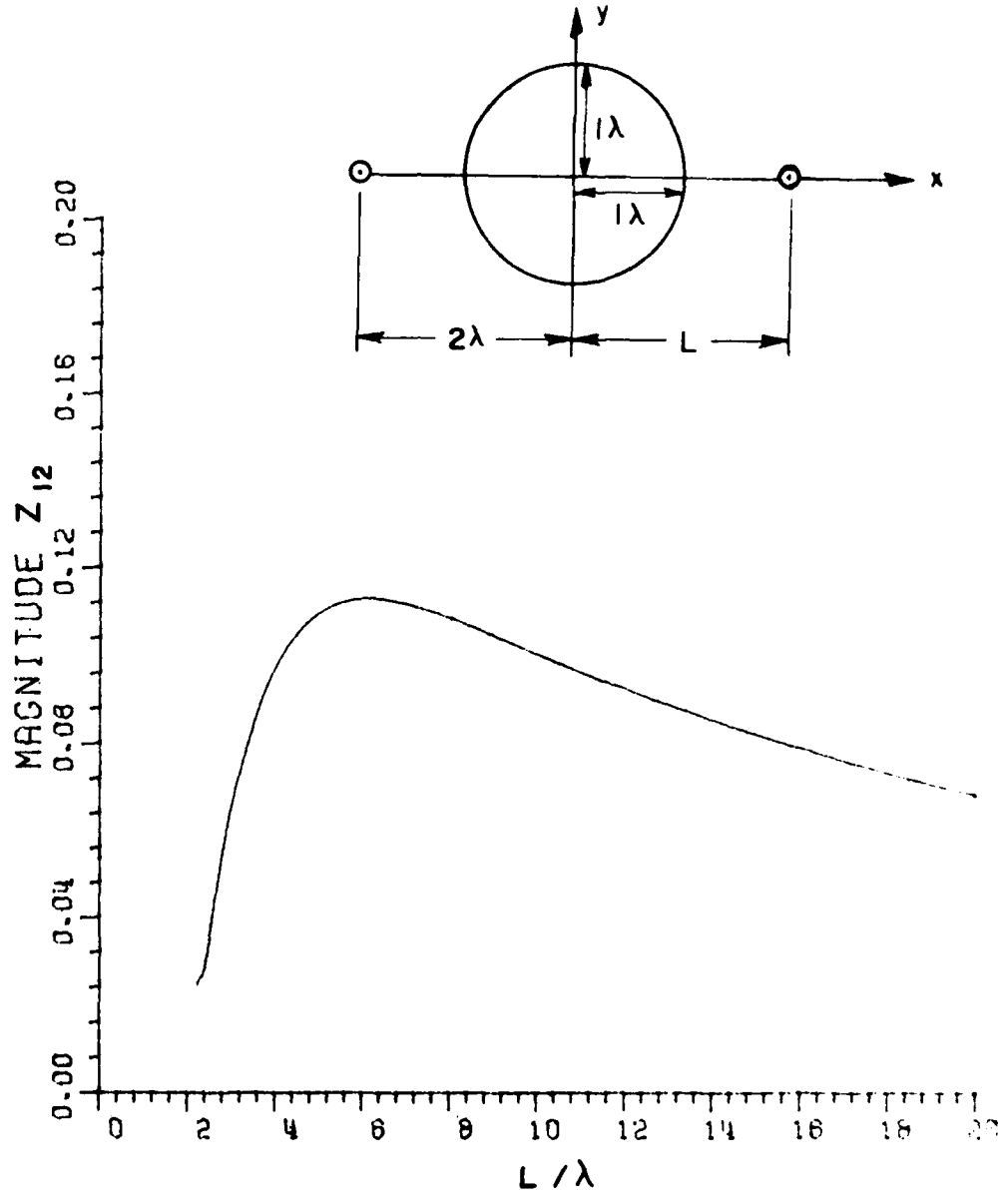

Figure 26. Coupling between two axial PWS dipoles near an infinite circular cylinder as one dipole moves along the x axis.

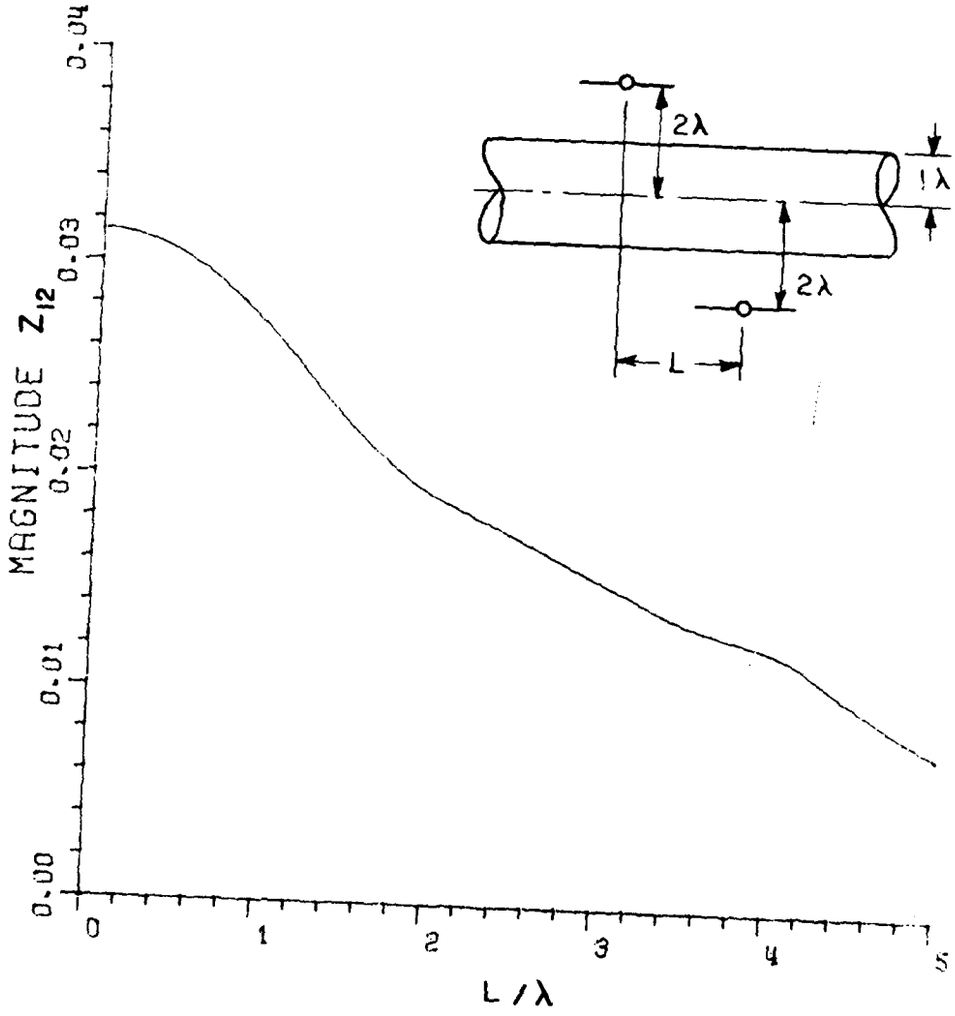

Figure 27. Comparison between two PWS dipoles as one dipole moves along the z axis.

CHAPTER VI
MONOPOLES ON CURVED SURFACES

The preceeding section presented a general method for computing the currents on thin wire antennas near a cylinder. A related problem of great interest is when the antenna is attached to the cylinder and driven against it. The simplest example of this is the case of a monopole which is normal to the surface at the attachment point.

It would be desirable to continue to employ the piecewise sinusoidal Galerkin method since the solution would be compatible with the hybrid method already presented. To accomplish this some difficulties must first be resolved.

The piecewise-sinusoidal functions are efficient because they are very similar to the actual current distribution on a wire. One of the most noteable features is that the current goes to zero (as expected) at the ends of the wire. When this wire is attached to a surface this is no longer true. Since the current is in general not zero at the feed point of a monopole special techniques will have to be developed in order to handle this problem.

A. Image Theory Solution

If the radius of curvature of the surface is large, then image theory can be used to compute the currents without difficulty. This case is shown in Figure 27. In this figure the wires have been broken up into segments and the corresponding PWS modes have been included and numbered for reference. Writing the equations of Figure 27 gives

$$\begin{aligned} v_1 &= Z_{11}I_1 + Z_{12}I_2 + Z_{13}I_3 + Z_{14}I_4 + Z_{15}I_5 + Z_{16}I_6 + Z_{17}I_7 \\ v_2 &= Z_{21}I_1 + Z_{22}I_2 \cdots \\ &\vdots \\ v_7 &= Z_{71}I_1 + Z_{72}I_2 \cdots Z_{77}I_7 \end{aligned} \tag{75}$$

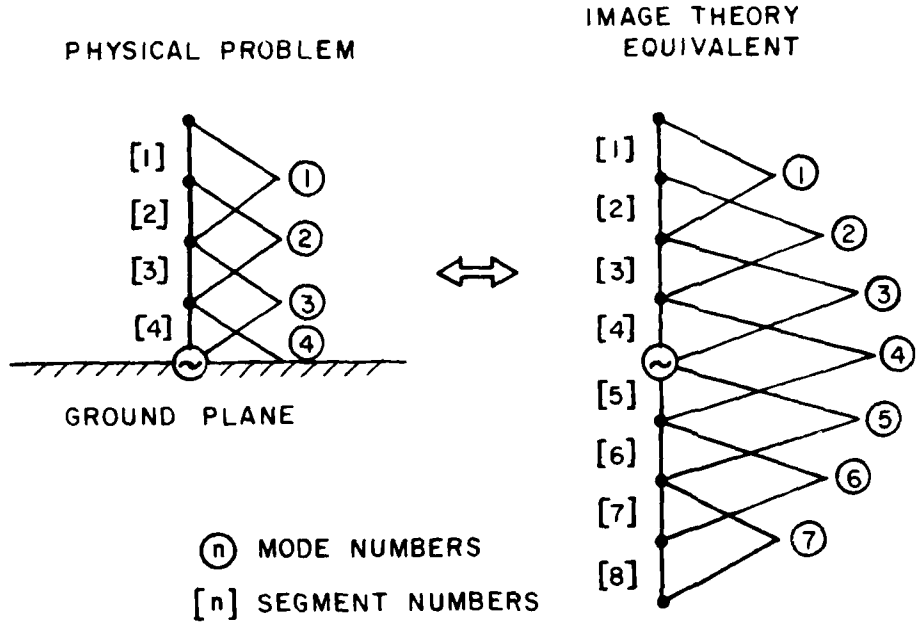

Figure 27. Example of the segments and mode structure on a monopole and its dipole image equivalent.

from symmetry it is known that

$$I_1 = I_7, \quad I_2 = I_6, \quad I_3 = I_5 \tag{76}$$

and thus in matrix form

$$[V] = \left\{ \begin{bmatrix} Z_{11} & Z_{12} & Z_{13} & Z_{14} \\ Z_{21} & Z_{22} & Z_{23} & Z_{24} \\ Z_{31} & Z_{32} & Z_{33} & Z_{34} \\ Z_{41} & Z_{42} & Z_{43} & Z_{44} \end{bmatrix} + \begin{bmatrix} Z_{17} & Z_{16} & Z_{15} & 0 \\ Z_{27} & Z_{26} & Z_{25} & 0 \\ Z_{37} & Z_{36} & Z_{35} & 0 \\ Z_{47} & Z_{46} & Z_{45} & 0 \end{bmatrix} \right\} [I] \tag{77}$$

or

$$[V] = \{[Z_F] + [\Delta Z]\}[I] \qquad (78)$$

Several important observations can be drawn from (78). First, the Z_F matrix is merely the standard impedance matrix which would be constructed if the antenna had been defined using only segments 1-5 in free space. Secondly, the $[\Delta Z]$ matrix consists of couplings only between modes on opposite sides of the ground plane. These couplings are the same as the coupling between modes in $[Z_F]$ if only reflected ray paths were considered since the modes below the ground plane are merely images of the segments above.

Thus instead of formulating the problem using image theory, the problem can be solved directly by computing a free space impedance matrix and a perturbation impedance matrix using reflection theory. This result is not too surprising when one considers the following. Each term Z_{mn} of the matrix [Z] is obtained by computing the coupling between a test dipole and an expansion dipole with no regard to the rest of the antenna. Thus except for the case where the test or expansion dipoles is in contact with the surface, the theory presented in Chapter IV would suffice. The discussion on image theory was necessary only to justify the existence of the mode which "straddles" the surface (mode 4) and to provide a means of including it in the current theory. The ground plane can be replaced by a curved surface as follows. Recall that each term (Z_{mn}) of the [Z] matrix represents the total coupling between dipole modes m and n, regardless of the structure of the rest of the antenna. Thus for modes near a curved surface this includes rays diffracted or reflected by the surface. If the radius of curvature of the surface is not large, then it is necessary to use GTD or GO in order to obtain an accurate result. The one exception to this is when one of the wire segments is quite near the surface and extremely short, then the surface still appears as a ground plane and image theory can be used. Thus in the case of a monopole, the [Z] matrix can be constructed using GO or GTD for all terms except for the mode which "straddles" the surface. This "straddling" mode can be adequately handled with image theory, with the restriction that it must be much shorter than the radius of the cylinder.

B. Numerical Implementation

Several problems were encountered when the above technique was used in a computer program. Consider the coupling between modes a and b which lie on a wire normal to the surface. In this case the reflection point is where a straight line extending the dipole to the cylinder would touch. Since GO or GTD only includes fields

transverse to the direction of propagation, the Z_{ab} term would be zero. This occurs because the field must be dotted with the direction of the segment. Since the direction of the segment is along the ray path, this dot product is zero. In practice, this problem is resolved by putting the test dipole on the surface of the wire and the expansion dipole along the center of the wire. This however raises two other questions.

First, since the wire is assumed to be round, the test dipole can be placed at any position on the outer surface without affecting the geometry with respect to the wire. However this affects the geometry of the two dipoles with respect to the curved surface. In fact the only cases where this placement does not have any effect is when the surface at the reflection point is spherical or planar. Numerical experiments with a thin wire normal to an elliptic cylinder were performed using the geometry in Figure 28. These results (Figures 29, 30) showed that for cylinders of reasonable size the slight change in geometry does affect the computed coupling, this effect was quite small. Thus the placement of the test dipole was arbitrarily chosen so that $\theta = 0^{o}$.

Another possible source of numerical error arises from the radial wire. One of the basic assumptions used to compute the coupling in this paper is that the wires are electrically thin. This is not a limitation of the moment method but a requirement imposed to simplify the computational problems. Since the wires are on the order of .006λ or less, the angle of incidence is quite small even for wires which are close to the surface. This would appear to pose great numerical problems. Again numerical experiments show that this generally does not lead to incorrect results. The reason for this is as follows. It is well known that the endfire field of a dipole is only significant in the near-field. Examination shows that as $\theta \rightarrow 0$, $E_{\rho} \rightarrow 0$ and E_z falls off as $1/R^2$, thus the field quickly dies away. Numerical results showed that for wire radii as small as .0005λ with 6 digit precision the field became negligibly small before numerical problems due to $\theta \rightarrow 0$ were encountered.

Another problem resulted from the tip of the mode which touched the surface, mode 3 in Figure 27. When the self-coupling of mode 3 is being computed, the distance from the source point (on the outside of the wire) and the observation point (on the axis of the wire) is quite small. Since the source point is a caustic, the field varies rapidly in this region. This rapidly changing field requires that the expansion mode (along the axis) be broken up into many integration points for the numerical integration to yield an accurate result.

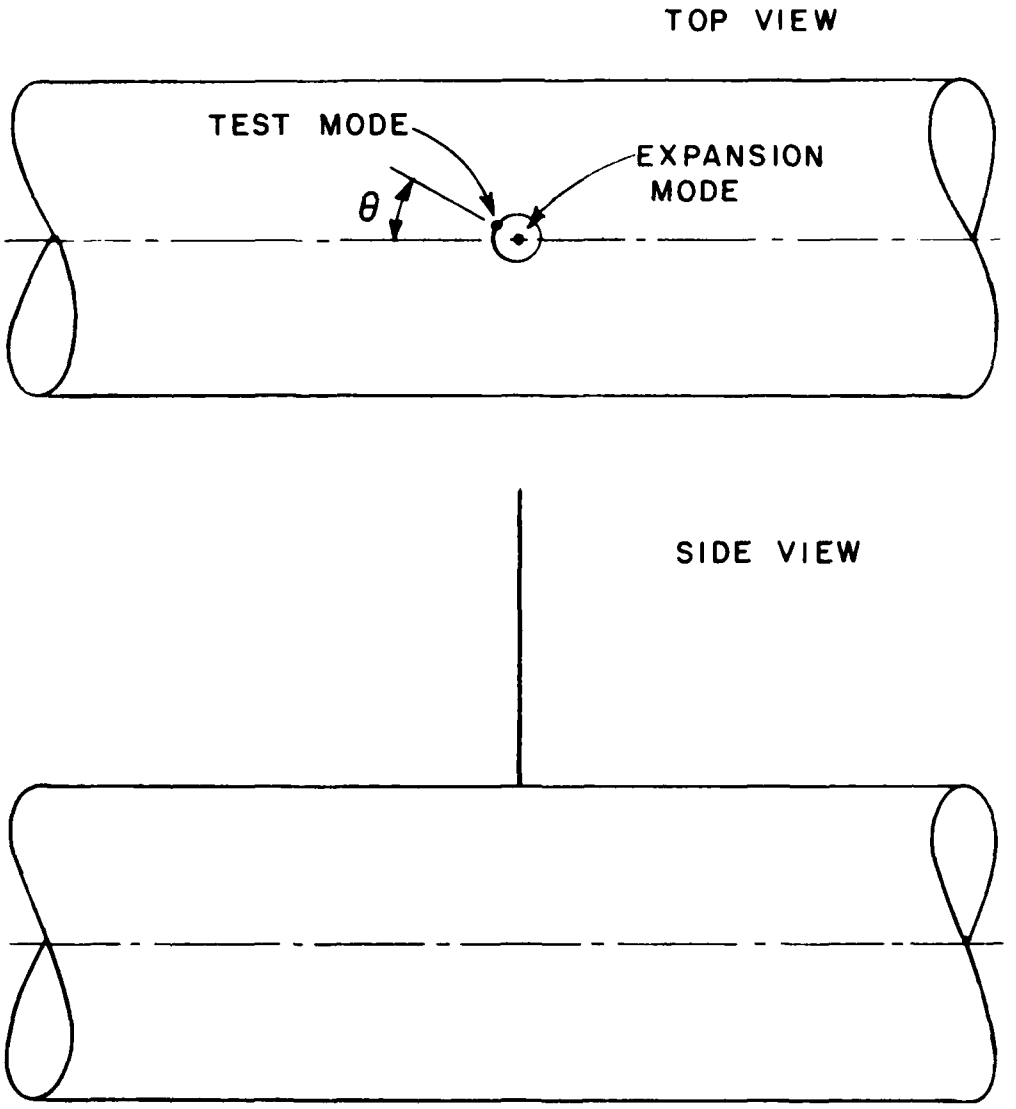

Figure 28. Location of the test and expansion dipoles on a thin wire mounted on a cylinder.

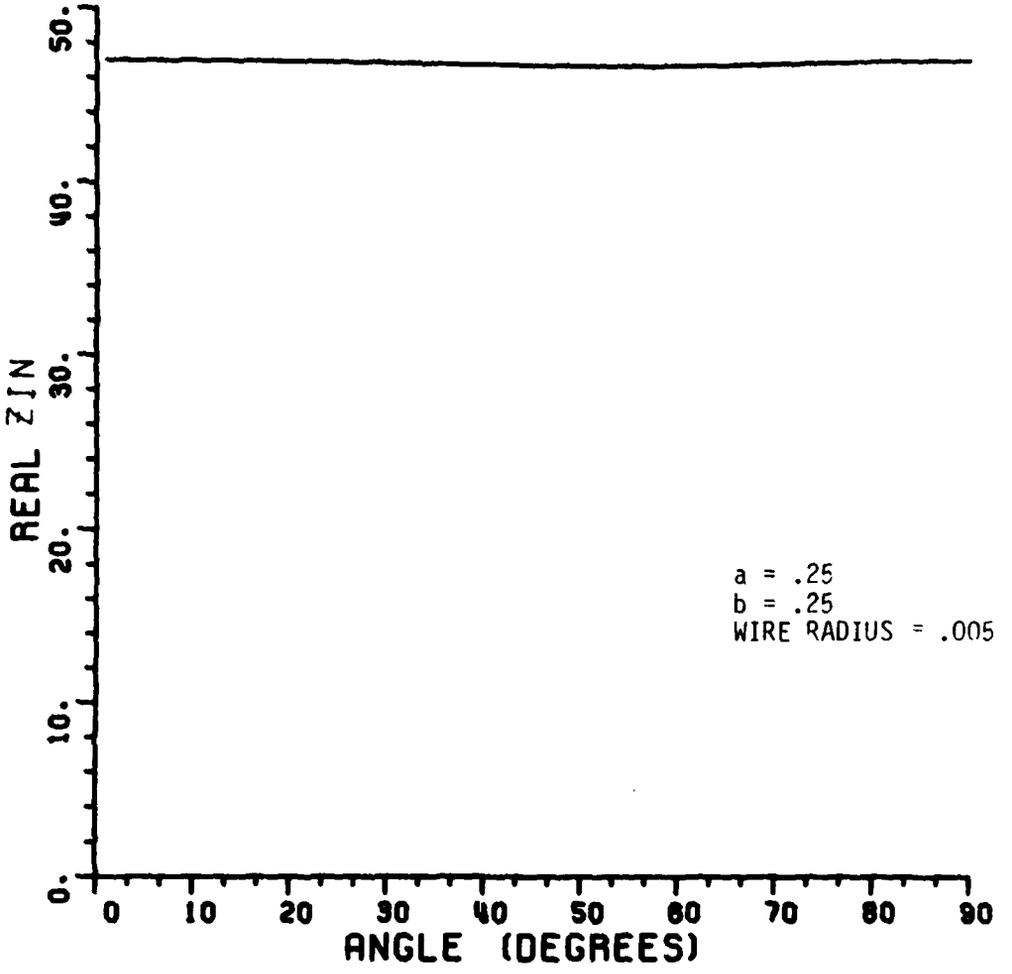

Figure 29. Real input impedance of a monopole as a function of the location (θ) of the test dipole.

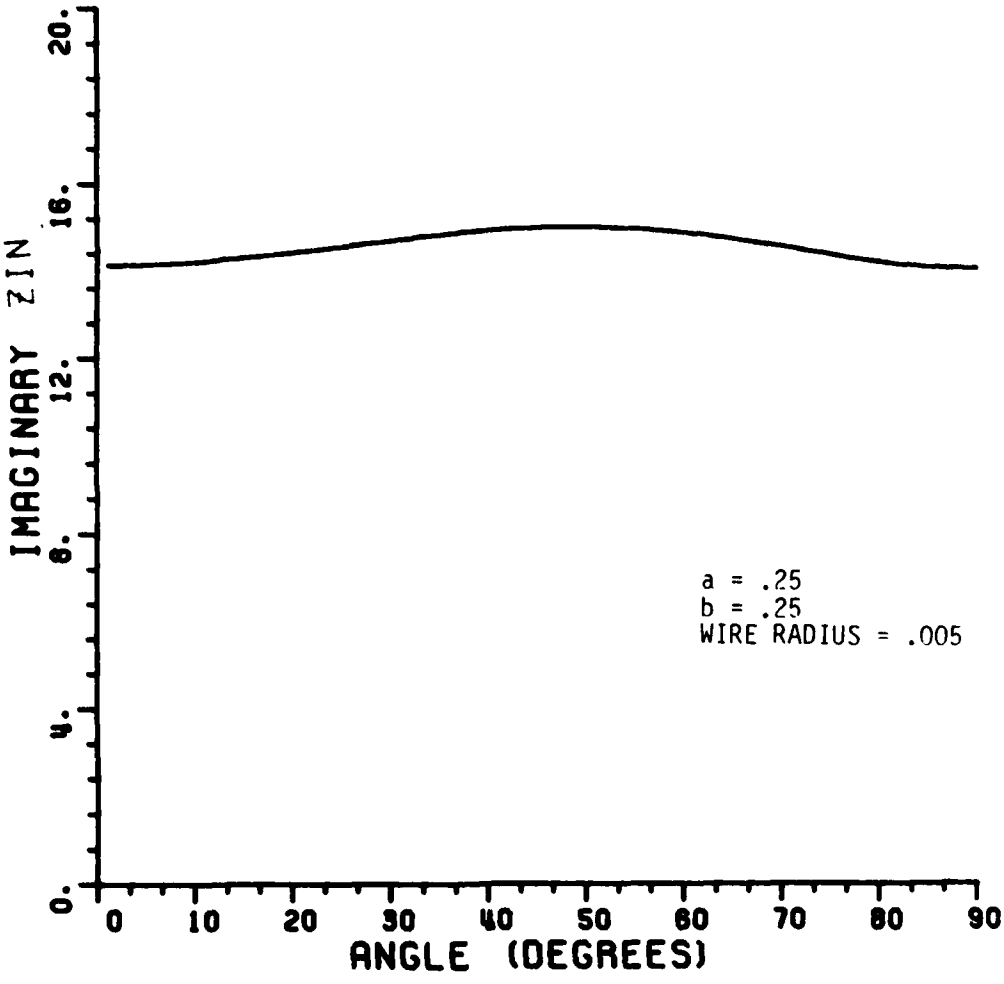

Figure 30. Complex input impedance of a monopole as a function of the location (θ) of the test dipole.

C. Results

Figures 31,32 show the computed input impedance of a monopole on a circular cylinder. The length was chosen such that the monopole is resonant when the cylinder becomes a flat ground plane. Figure 33 shows how the hybrid technique compares with experimental data supplied by Wang [14]. Note that except for the classical resonance shift the curves "track" well.

While the image theory solution of the monopole problem gives accurate results, it has the drawback of requiring that one mode "straddle" the surface. This mode also has a length restriction which usually increases the number of required segments. Finally it is a non-physical situation and thus is difficult to work with on an intuitive basis. These difficulties could hinder future work. Because of these problems an alternate technique referred to as the half mode solution was developed which alleviated the above problems.

D. Half Mode Solution

This solution sets up only half of the mode that originally "straddled" the surface. The couplings computed as a result of this half mode are not valid until the $[Z_F]$ and $[\Delta Z]$ impedance matrices are added together to produce the total impedance matrix [Z].

As stated earlier, the coupling between two PWS dipoles is actually computed via the coupling between four PWS monopoles. These couplings are indicated as arrows in Figure 34. The point charge (due to the non-zero current at one end) that would result from each monopole is neglected since it will be cancelled out when these monopoles are connected as dipoles. Now consider the coupling between a PWS dipole and a PWS monopole on a ground plane in Figure 35 where the image theory couplings have been shown as dotted lines. Observe that via image theory, this is identical to the coupling between two dipoles, but without explicitly defining the image arm of the monopole. This forms the basis by which the half mode solution works. Careful examination shows that this is just a logical extension of the image theory solution. Thus it was not necessary to define all of the mode that straddled the surface but only the portion above. The only modification being, any coupling between half-modes (i.e., monopoles on the surface) must be doubled to convert them to dipole-dipole couplings.

The two impedance matrices generated by this method have a peculiar quality which can be explained as follows. Letting the half mode of Figure 35 be labeled x and the dipole mode be labeled y, the following observation can be made. The terms z_{xy} and z_{yz} of the matrix $[Z_F]$ are not valid by themselves (i.e., without adding

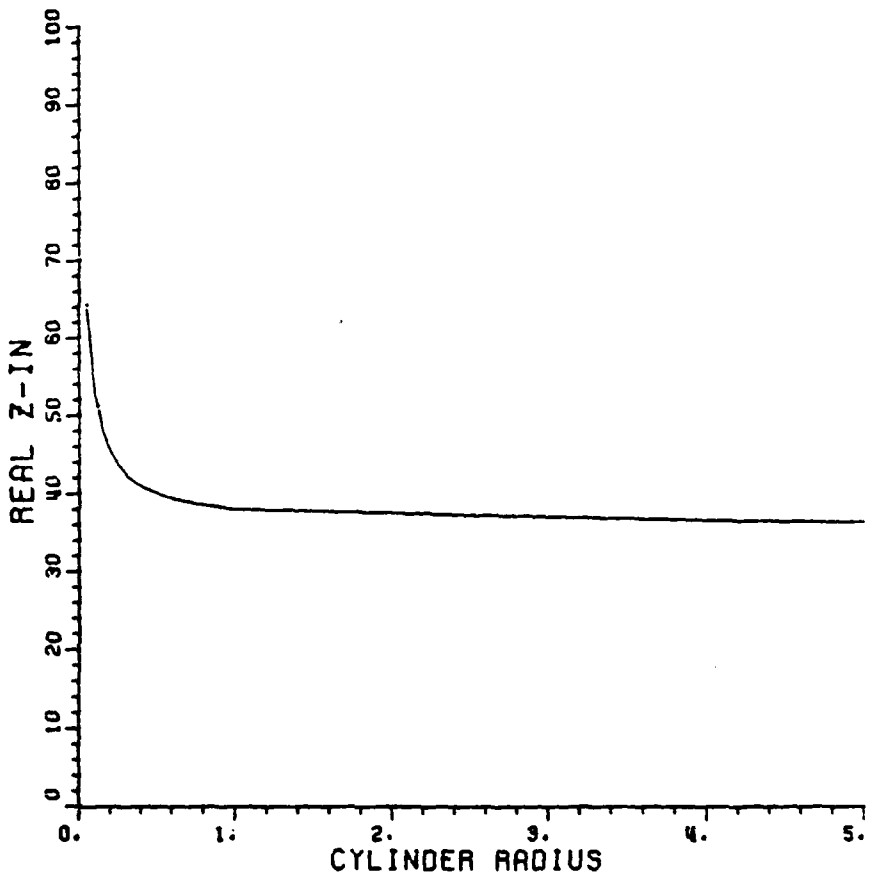

Figure 31. Real input impedance of a quarter wave monopole mounted on an infinite circular cylinder.

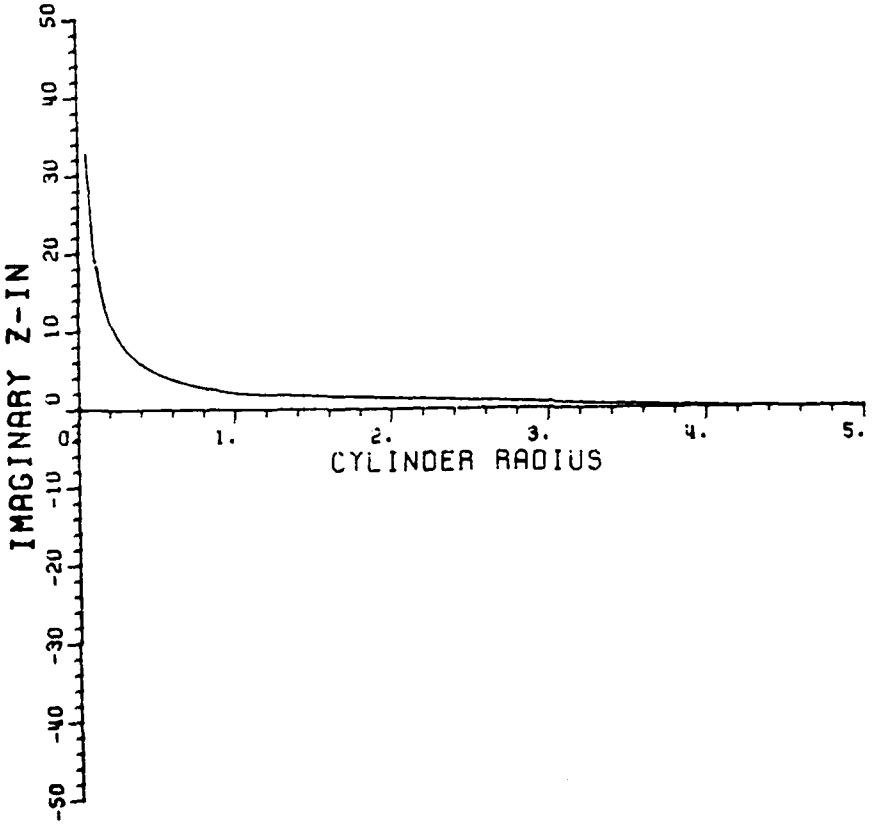

Figure 32. Imaginary input impedance of a quarter wave monopole mounted on an infinite circular cylinder.

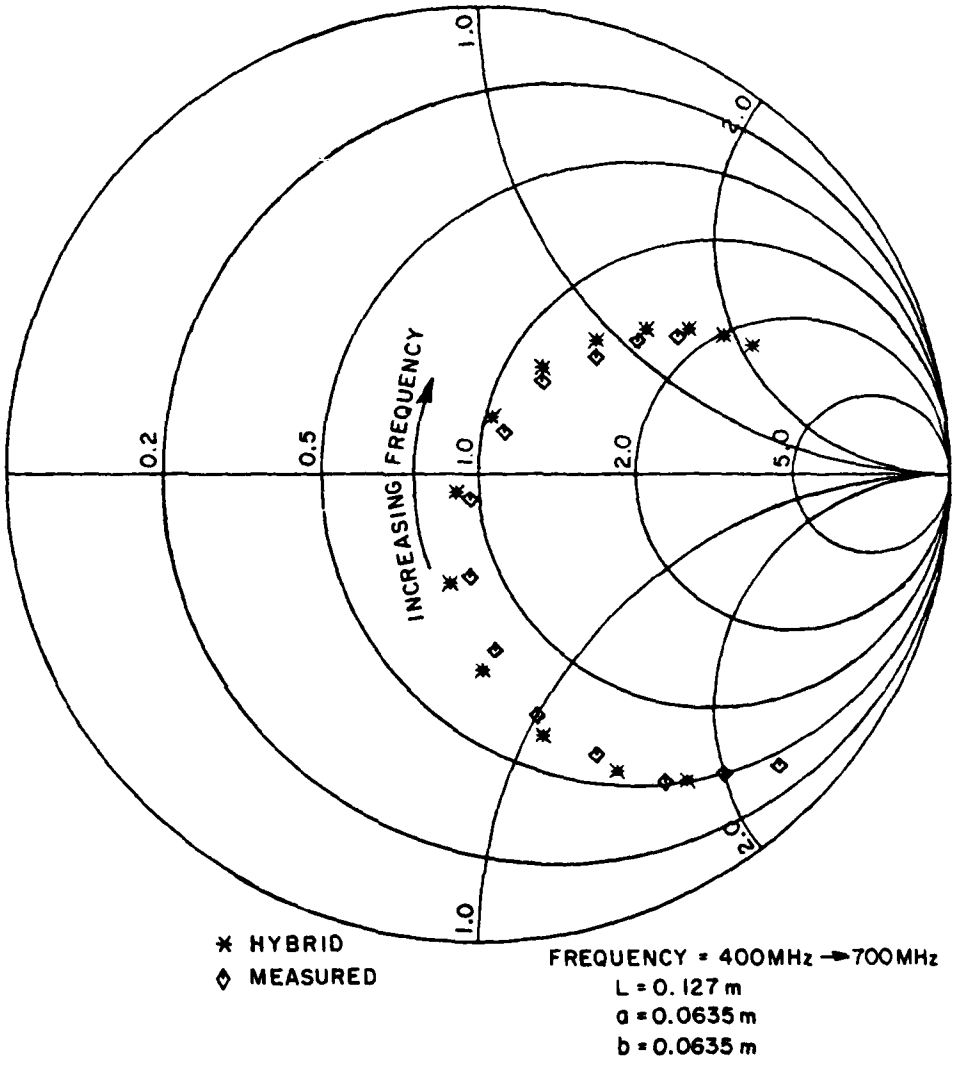

Figure 33. Calculated and measured input impedance of a monopole on an infinite cylinder.

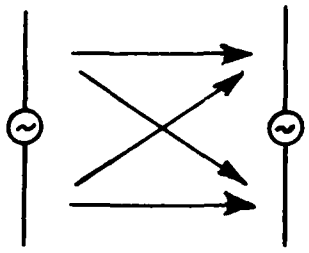

Figure 34. Graphical representation of the monopole-monopole couplings required for a dipole-dipole coupling.

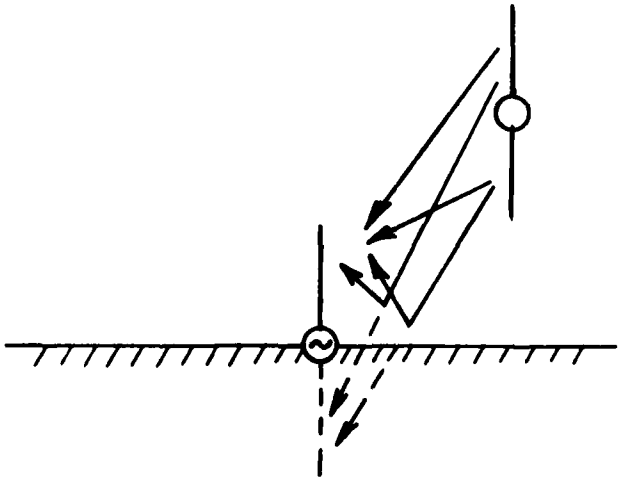

Figure 35. Image equivalent of Figure 34.

Δz_{yx} or Δz_{xy}). This arises because each term in $[Z_F]$ is by definition a dipole to dipole impedance but z_{xy} and z_{yx} are monopole-dipole impedances (without the point charge contribution). However since Δz_{xy} and Δz_{yx} contain the corresponding monopole-dipole impedances (again without point charge contribution) their sum does define a dipole-dipole impedance this giving v valid impedance matrix. The computer programs used to generate the half mode solution were changed to construct a solution using the half-mode technique. The results were identical (within numerical error) to those produced by the image-theory solution. The drawback to this method is that it is not directly compatible with Richmond's thin wire programs. These routines were never intended to be used on a system where such a mode could exist and thus they would have to be changed. For the purposes of this report, the half mode solution was only implemented well enough to run a few cases and demonstrate that it would work. The solution was presented only as a stepping stone to future work in this field.

CHAPTER VII
SUMMARY AND CONCLUSION

The hybrid technique of Ekelman has been expanded to handle a more general set of thin wire antennas and scatterers than was previously possible. The uniform GTD of Pathak et al. [3]was used to provide a means of analyzing systems where antennas are arbitrarily oriented near an infinite, perfectly-conducting elliptic cylinder, and a new hybrid image theory technique was developed to analyze monopoles mounted on the cylinder. Both of these new solutions retain the format and conventions set up by Richmond and are completely compatible with his powerful moment-method computer code.

The free space impedance matrix was computed using the conventional moment method technique. A perturbation matrix, called the delta impedance matrix after Thiele et al. was then added to the free space matrix. This delta matrix, contained the coupling between elements due to GTD type rays which were reflected or diffracted by the cylinder. Thus the effects of the cylinder were accounted for in the final solution.

The first problem solved was that of the piecewise sinusoidal dipoles in the presence of the aforementioned cylinder. A dipole with a single PWS current distribution is the single most important type of antenna that can be considered since each element of the impedance matrix is merely the coupling between two such dipoles. The solution obtained was shown to be accurate by comparing it with three independent techniques. The NEC Basic Scattering Code developed at The Ohio State University was used to check general orientations in the far field results. A moment method eigenfunction technique was used to check the results when both dipoles were in the near field. The eigenfunction solution had problems in the deep shadow region so measured data was used to check that case. All of the independent results showed the hybrid method to be accurate and reliable.

The second class of problem solved was a monopole mounted on a curved surface. The solution was obtained by image theory with perturbations of the images by the curved surface. This solution is very general and is applicable to any curved or flat surface. To demonstrate its usefulness, the monopole was put on an infinite,

perfectly conducting elliptic cylinder and its input impedance was obtained. This computed impedance was shown to agree favorably with measured data. A second method called the half-mode solution was also presented for solving the monopole problem. This method used the same theory as the original but in a manner which could make future work easier. While the half-mode solution was explained fully, it was intended only to present a possible alternative. The implementation was carried only far enough to demonstrate that it will work. More work will need to be done if the full potential of this method is to be realized.

REFERENCES

1. Ernest P. Ekelman, Jr., "A Hybrid Technique for Combining the Moment Method Treatment of Wire Antennas with the GTD for Curved Surfaces", Ph.D. Dissertation, The Ohio State University, 1978.

2. R. J. Marhefka, "Analysis of Aircraft Wing-Mounted Antenna Patterns", Report 2902-25, June 1976, The Ohio State University ElectroScience Laboratory, Department of Electrical Engineering; prepared under Grant NGL 36-008-138 for National Aeronautics and Space Administration.

3. P. H. Pathak, W. D. Burnside and R. J. Marhefka, "A Uniform GTD Analysis of the Scattering of Electromagnetic Waves by a Smooth Convex Surface", Report 784583-4, April 1979, The Ohio State University ElectroScience Laboratory, Department of Electrical Engineering; prepared under Contrac N62269-78-C-0554 for Naval Air Development Center.

4. R. G. Kouyoumjian and P. Pathak, "A Uniform Geometrical Theory of Diffraction for an Edge of a Perfectly Conducting Surface", Proc. of the IEEE, Vol. 62, No. 11, November, 1974, pp. 1448-1461.

5. F. W. Schmidt and R. J. Marhefka, "Numerical Electromagnetic Code (NEC) - Basic Scattering Code. Part II: Code Manual", Report 784508-14, September 1979, The Ohio State University ElectroScience Laboratory, Department of Electrical Engineering; prepared under Contract N00123-76-C-1371 for Naval Regional Procurement Office.

6. N. A. Logan, "General Research in Diffraction Theory", Vol. I, LMSC-288087; and Vol. II, LMSC-2588088, Missiles and Space Division, Lockheed Aircraft Corp., 1959.

7. G. A. Thiele and T. M. Newhouse, "A Hybrid Technique for Combining Moment Methods with the Geometrical Theory of Diffraction", IEEE Trans. on Antennas and Propagation, Vol. AP-23, No. 1, January 1975.

8. J. H. Richmond, "Radiation and Scattering by Thin-Wire Structures in the Complex Frequency Domain", Report 2902-10, July 1973, The Ohio State University ElectroScience Laboratory, Department of Electrical Engineering; prepared under Grant

NGL 36-008-138 for National Aeronautics and Space Administration, (NASA-CR-2396).

9. W. L. Stutzman and G. A. Thiele, Modern Antenna Theory, John Wiley and Sons, New York, 1979 (to be published).

10. J. H. Richmond, "Computer Program for Thin-Wire Structures in a Homogeneous Conducting Medium", National Technical Information Service, Springfield, VA 22131, NASA Contractor Report CR-2399.

11. V. H. Rumsey, "The Reaction Concept in Electromagnetic Theory", Physical Review, Ser. 2, Vol. 94, June 1954.

12. R. J. Marhefka and W. D. Burnside, "Numerical Electromagnetic Code (NEC) - Basic Scattering Code. Part I: User's Manual," Report 784508-18, September 1979, The Ohio State University ElectroScience Laboratory, Department of Electrical Engineering; prepared under Contract N00123-76-C-1371 for Naval Regional Procurement Office, Long Beach, California.

13. L. Ersoy and N. Wang, "Surface Current and Charge Density Induced on an Infinite, Perfectly-Conducting Circular Cylinder in the Presence of Finite Axial Thin Wire - Transverse Magnetic Code," Report 4172-2, June 1977, The Ohio State University ElectroScience Laboratory, Department of Electrical Engineering; prepared under Contract F29601-75-C-0086 for Kirtland Air Force Base, NM.

14. N. Wang, personal communication.

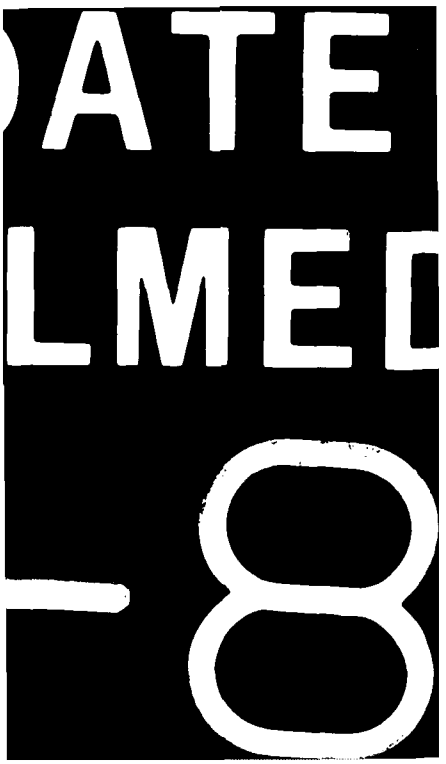
ATE
LMED
8